Observed Relationships between Supercell Mesocyclone Intensity and Evolution, Background Environmental Characteristics, and Cell Mergers

MATTHEW D. FLOURNOY,[a,b] ANTHONY W. LYZA,[c] ANDREW R. WADE,[c,a] AND JANNICK FISCHER[d]

[a] *NOAA/NWS/NCEP Storm Prediction Center, Norman, Oklahoma*
[b] *School of Meteorology, University of Oklahoma, Norman, Oklahoma*
[c] *Cooperative Institute for Severe and High-Impact Weather Research and Operations, University of Oklahoma, Norman, Oklahoma*
[d] *Department Troposphere Research, Karlsruhe Institute of Technology, Karlsruhe, Germany*

(Manuscript received 11 September 2023, in final form 10 May 2024, accepted 30 May 2024)

ABSTRACT: Cell mergers with supercells are relatively common, but much remains unknown about how they may influence subsequent supercell hazards. Furthermore, many outstanding questions regarding mesocyclone evolution exist despite numerous studies linking supercell hazards with the background environments in which they occur. In this study, we analyze the Multi-Year Reanalysis of Remotely Sensed Storms dataset along with hundreds of observed supercell tracks to begin addressing these ideas. In line with recent studies, the outcome of a supercell–cell merger (specifically the final strength of the low-level supercell mesocyclone) is not strongly related to the background environment. Of the parameters that we tested, mixed-layer (ML) LCL exhibited the largest correlation, but the very small coefficient of determination suggests limited operational use. More significantly, the incorporation of Storm Prediction Center objective analyses yields novel quantification of observed mesocyclone strengths in different environments. Of the environmental characteristics tested, kinematic parameters like 0–3-km storm-relative helicity (SRH) and 0–3-km bulk wind difference are more correlated with peak mesocyclone intensity than thermodynamic variables like CAPE and CIN. 0–3-km SRH exhibits the largest correlation, and its variability explains roughly one-third of the variance of peak azimuthal shear. We show trends in peak mesocyclone intensity across notable environmental parameter spaces, as well as how low-level mesocyclone strength fluctuates as background environmental characteristics evolve. Environmental trends during and preceding the times of peak mesocyclone strength are quantified. These analyses may be useful for predicting short-term mesocyclone intensity changes in real time.

SIGNIFICANCE STATEMENT: This study addresses open research questions related to how storms merging with supercell thunderstorms may influence supercell evolution and how supercells tend to evolve in different background environments. We find that an environmental measure of cloud-base height is statistically correlated with whether a supercell–cell merger will yield a strengthening or weakening supercell, but the strength of this correlation is quite weak. We find stronger correlations between peak supercell strength across storm lifetimes and some environmental characteristics, particularly parameters related to the change in the wind with height in the lowest few kilometers above ground level. These relationships may be useful for predicting short-term changes in supercell strength in real time.

KEYWORDS: Severe storms; Storm environments; Supercells

1. Introduction

The defining characteristic of a supercell thunderstorm is the mesocyclone: a rotating updraft around 2–10 km wide that persists for around 1 h or more [American Meteorological Society (AMS) Glossary]. The strength of the mesocyclone influences the intensity of supercell hazards, including damaging surface winds (e.g., Smith et al. 2012), tornadoes (e.g., Markowski and Richardson 2014), hail (e.g., Dennis and Kumjian 2017), and excessive rainfall (e.g., Nielsen and Schumacher 2018). The mesocyclone's vertical vorticity predominantly stems from the tilting—by an updraft—of initially horizontal vorticity in the background environment (Rotunno and Klemp 1982, 1985; Davies-Jones 1984; Dahl 2017; Coffer et al. 2023). Hence, relating the intensity of the mesocyclone to the background environment is useful for extended-range supercell prediction (e.g., Rasmussen and Blanchard 1998; Thompson et al. 2003). However, not all mesocyclones that form within the same general background environment behave identically. Recent modeling work highlighted the storm-scale variability that can occur in virtually the same environments (Coffer et al. 2017; Flournoy et al. 2020; Markowski 2020; Hutson and Weiss 2023). While some environments seem to set a baseline simulated storm intensity (e.g., the near-field tornadic supercell ensemble in Coffer et al. 2017), essentially negligible changes to the homogeneous base state can yield different outcomes, at least in terms of surface vortex production (e.g., the near-field nontornadic ensemble in Coffer et al. 2017 or the far-field tornadic ensemble in Flournoy et al. 2020). In the real atmosphere, small-scale features such as cell mergers (e.g., Klees et al. 2016; Lyza and Flournoy 2023), boundaries (e.g., Magee and Davenport 2020; Wilson et al. 2023), and terrain-induced flows

Fluornoy's current affiliation: NOAA/National Severe Storms Laboratory, Norman, Oklahoma.
Lyza's current affiliation: NOAA/National Severe Storms Laboratory, Norman, Oklahoma.

Corresponding author: Matthew Flournoy, matthew.flournoy@noaa.gov

DOI: 10.1175/MWR-D-23-0199.1

(e.g., Lyza and Knupp 2018; Lyza et al. 2020; Katona and Markowski 2021) can cause different evolutionary paths between neighboring supercells. As such, better understanding and anticipation of processes influencing observed supercell mesocyclone evolution is an active goal of the community.

Better understanding the influence of cell mergers on supercell evolution, including tornado production, is a tantalizing topic given its possible efficient integration into real-time forecasting. Much of our knowledge of these processes stems from case studies of observed cell mergers with supercells. In some cases, mergers were associated with brief intensification periods and tornadogenesis (Wurman et al. 2007; Edwards and Thompson 2024) and in others with overall supercell weakening (e.g., Klees et al. 2016). A couple climatological studies noted the tendency for tornadogenesis periods (e.g., defined as the 30-min time frame within 15 mins before or after tornadogenesis) to feature more mergers than nontornadogenesis periods (e.g., Lee et al. 2006; Rogers and Weiss 2008; Lyza and Flournoy 2023). These studies featured a range of convective modes and tornado damage ratings. However, when analyzing significant tornado events, Rogers (2012) found that only around a quarter of tornadogenesis periods featured mergers. Lyza and Flournoy (2023) also showed that, during the supercell-tornado outbreak of 27–28 April 2011, longer-lived tornadoes (with lifetimes of 1 h or more) tended to feature less mergers during the tornadogenesis period than shorter-lived tornadoes. These findings suggest that in environments supportive of tornado production, tornadogenesis windows featuring less cell mergers may be more likely to yield longer-lived, stronger tornadoes. However, these studies also clearly show that the influence of cell mergers on supercell evolution and tornado production is complex and difficult to anticipate in real time.

Part of the reason for this complexity seems to be the wide range of interactions that can occur between cell mergers and supercell structures. Some numerical studies show that mergers may favorably modify the mesocyclone vorticity budget, perhaps via increased baroclinic vorticity generation in the rear flank (e.g., Hastings et al. 2014), greater upward forcing and vorticity tilting along colliding outflow boundaries (e.g., Tanamachi et al. 2015), or enhanced outflow yielding longer residence times beneath the low-level updraft (e.g., Fischer and Dahl 2023). Conversely, negative impacts to the primary supercell could occur via increased hydrometeor loading in the low- and midlevel updrafts (e.g., Klees et al. 2016), increasingly rain-cooled air yielding detrimentally buoyant rear-flank outflow or forward-flank inflow (e.g., Markowski et al. 2002; Kumjian 2011), and/or perhaps kinematic disruptions to vorticity-rich mesocyclone inflow on the left flank (e.g., Klees et al. 2016). Regardless, how the primary supercell evolves is clearly highly dependent on the supercell-relative location and orientation of the merging cell (e.g., Jewett et al. 2006; Hastings and Richardson 2016; Lyza and Flournoy 2023).

In light of these complexities, a trio of recent studies attempted to generalize how supercell mesocyclones may evolve when cell mergers occur (Flournoy et al. 2022; Lyza and Flournoy 2023; Fischer et al. 2023; hereafter F22, LF23, and F23, respectively). One primary finding from F22 and LF23 was that weaker mesocyclones tended to strengthen during cell merger events and vice versa for stronger mesocyclones. A cell merger "event" in these studies comprised one or more individual cell mergers, which were grouped into "events" when individual mergers occurred within 30 min of each other. This result was drawn from observational analysis of two different datasets, including a climatological perspective of 342 supercells occurring from 2003 to 2011 (including the 27 April 2011 event, F22) and a focused examination of the 29 tornadic supercells that occurred during the 27 April 2011 event (LF23). In a collaborative comment on these studies, F23 reanalyzed the observations from F22 and LF23, as well as a separate group of 122 supercells from 2010 to 2011. Based on the reanalysis, the tendency for weaker mesocyclones to strengthen and stronger mesocyclones to weaken exists across the entire supercell life cycle, not just during cell merger periods. In other words, an inverse relationship generally exists between initial mesocyclone intensity and the subsequent 30-min change in intensity during all phases of a supercell's life cycle.

This result suggests that mature supercell mesocyclones may tend to regress toward some mean intensity over their lifetimes. This is not a novel idea; it is well known that supercells (at least the ones that are discrete for their entire lifetimes) tend to exhibit an initial strengthening period, a mature, quasi-steady-state period, and a final weakening period (e.g., Bunkers et al. 2006; Coniglio and Parker 2020; Flournoy et al. 2021). The mature period may feature cyclic mesocyclone behavior that can contribute to relatively weaker and stronger periods, particularly at lower altitudes (e.g., Adlerman et al. 1999; Dowell and Bluestein 2002a,b). Supercells that produce increasingly significant hazards tend to inhabit environments with more favorable (hazard dependent) parameters; e.g., for increasing significant tornado potential, these include increased vertical wind shear, moister boundary layers, and greater low-level storm-relative flow (e.g., Rasmussen and Blanchard 1998; Thompson et al. 2003; Craven and Brooks 2004; Parker 2014; Coniglio and Parker 2020; Davenport 2021). Using a suite of base-state wind profiles, Goldacker and Parker (2021) quantified relationships between environmental shear characteristics and simulated mesocyclone intensity. The strongest low-level mesocyclones (i.e., having undergone a "low-level dynamical response") were associated with large 0–500-m storm-relative helicity (SRH) and streamwise vorticity, but not all environments in this parameter space yielded the dynamical response. No observational complement has been attempted to quantify any relationships between environmental parameters and observed, quantifiable mesocyclone intensity. This idea—as well as the need for an environmentally constrained analysis of cell mergers and mesocyclone evolution as noted in F22, LF23, and F23—motivates this study. We address the following related questions:

- Do supercell mesocyclones tend to regress toward a particular intensity? If so, over what time scales does this occur?
- Are mean mesocyclone intensities influenced by the background environment?
- Is mesocyclone evolution more strongly influenced by cell mergers in different environments?

We address these questions by synthesizing the F22 supercell dataset with the Storm Prediction Center's Surface

Objective Analysis (SFCOA) database to extract environmental profiles near each storm. In the ensuing analysis, we will show a general mean low-level mesocyclone intensity across environments, as well as how peak intensities vary as different environmental parameters change. We also reexamine possible relationships between cell mergers and subsequent low-level mesocyclone evolution and how these relationships may change in different background environments.

2. Data and methods

a. Summary of the F22 supercell dataset

The subsequent analysis relies on the dataset of supercell tracks analyzed in F22. This dataset includes 342 tornadic and significant-severe supercells that occurred between 2003 and 2011 in the contiguous United States. The events were drawn from the comprehensive database presented in Smith et al. (2012), which were then filtered to only include storms that produced at least one significant-severe report within 20–40 km from a WSR-88D site. Any candidate storms were then tracked for the period of time in which they remained within 75 km of a radar site. This was done to ensure sufficient sampling of the low-level mesocyclone by the nearest radar. These observations were incorporated into the reanalysis dataset used to characterize low-level mesocyclone intensity, Multi-Year Reanalysis of Remotely Sensed Storms (MYRORSS; Williams et al. 2022). Observations of MYRORSS maximum 0–3 km AGL azimuthal shear (referred to as "AzShear") were obtained to derive time series of low-level mesocyclone intensity for each supercell. The AzShear field is derived from applying a linear least squares derivative to the radar-derived velocities (Mahalik et al. 2019), yielding a grid with 0.005° (~500 m) horizontal spacing. All AzShear observations in the lowest 3 km are synthesized from up to the four closest radar sites (within 400 km), and the maximum value from that distribution is recorded as the maximum 0–3-km AzShear at that point. The mesocyclone intensity time series were created by recording the local maximum in AzShear (within a 10-km-wide search box centered on the storm) for each supercell roughly every 5 min. Unless otherwise stated, we use "mesocyclone" to specifically refer to the "low-level mesocyclone," as opposed to "near-surface" or "midlevel" circulations, for the remainder of the paper. The same is true for AzShear, which always refers to the 0–3-km maximum AzShear product.

Cell mergers along each supercell track were subjectively identified by the F22 authors. This involved intensive, manual analysis of WSR-88D observations along each supercell track. Individual cell mergers were recorded when the core of a discrete cell containing >35 dBZ on the lowest elevation scan merged with the core of the primary supercell. As in F22, cell merger events were then derived from the time series of individual cell mergers, with an event encompassing all individual mergers that occurred for an individual storm within 30 min of each other. The 30-min threshold applied to each individual merger in succession, such that a single merger event could be longer than 30 min in duration. We use this definition of a cell merger event for the analysis presented in section 5. Interested readers are referred to F22 for additional details regarding the construction of the supercell–cell merger dataset.

b. SFCOA environmental reanalysis

We used the SFCOA database (e.g., Bothwell et al. 2002; Thompson et al. 2007; Coniglio 2012) developed at the Storm Prediction Center to synthesize environmental information with the aforementioned supercell tracks. SFCOA is an hourly Rapid Update Cycle (RUC)-based reanalysis product that blends surface observations (primarily METAR and marine) with three-dimensional RUC analyses. The observations are analyzed on a 40-km grid using a two-pass Barnes scheme (Barnes 1973) before merging onto the 40-km RUC grid. Essentially, the surface objective analyses replace the RUC surface fields, yielding a more accurate depiction of the atmosphere every hour. Archived RUC data, which are available from 2005 to 2011 on isentropic–sigma hybrid vertical levels every 25 hPa, are used for all vertical levels above the SFCOA surface fields. In this study, SFCOA profiles are extracted every hour along each supercell track in the F22 dataset from 2005 to 2011. The profiles are extracted at the SFCOA grid point closest to the mesocyclone of interest at each hour; given the temporal and spatial resolutions of the storm tracks and SFCOA grid, respectively, the hourly profiles were extracted no more than 20–25 km from the observed mesocyclone location. These profiles and the ensuing analysis are presented in section 4.

3. Time scales of mesocyclone evolution

Before examining how mesocyclone intensity and evolution are related to environmental and merger characteristics, we first use this dataset to reexamine general trends in mesocyclone intensity using the MYRORSS AzShear observations. This helps provide a baseline understanding of how mesocyclone intensity generally varies across different environments, prior to examining influences from the environment and cell mergers in the next section. The findings of F22, LF23, and F23 show that initial mesocyclone intensity and the subsequent 30-min change in intensity are inversely related during any portion of the supercell's life cycle. These trends are evident over a large range of mesocyclone intensities, suggesting that the relationship is generally meaningful for observed supercells. To test how sensitive the result may be to the randomly extracted distribution of portions of supercell life cycles, we examined linear regressions between 1) AzShear evolution during 5–120-min intervals and 2) the initial AzShear at the start of said time interval. Examples of this are shown in Fig. 1a, where the scatter points for randomly selected 15- and 90-min periods of supercell life cycles are shown. The linear least squares regressions for both distributions reveal a negative slope along with a positive x intercept (indicating that there is a transition from strengthening to weakening mesocyclones at some point, not solely strengthening or weakening mesocyclones). The relationship is stronger over 90-min time periods than 15-min ones; e.g., over longer time periods, initially weaker mesocyclones are more likely to strengthen than over shorter time periods.

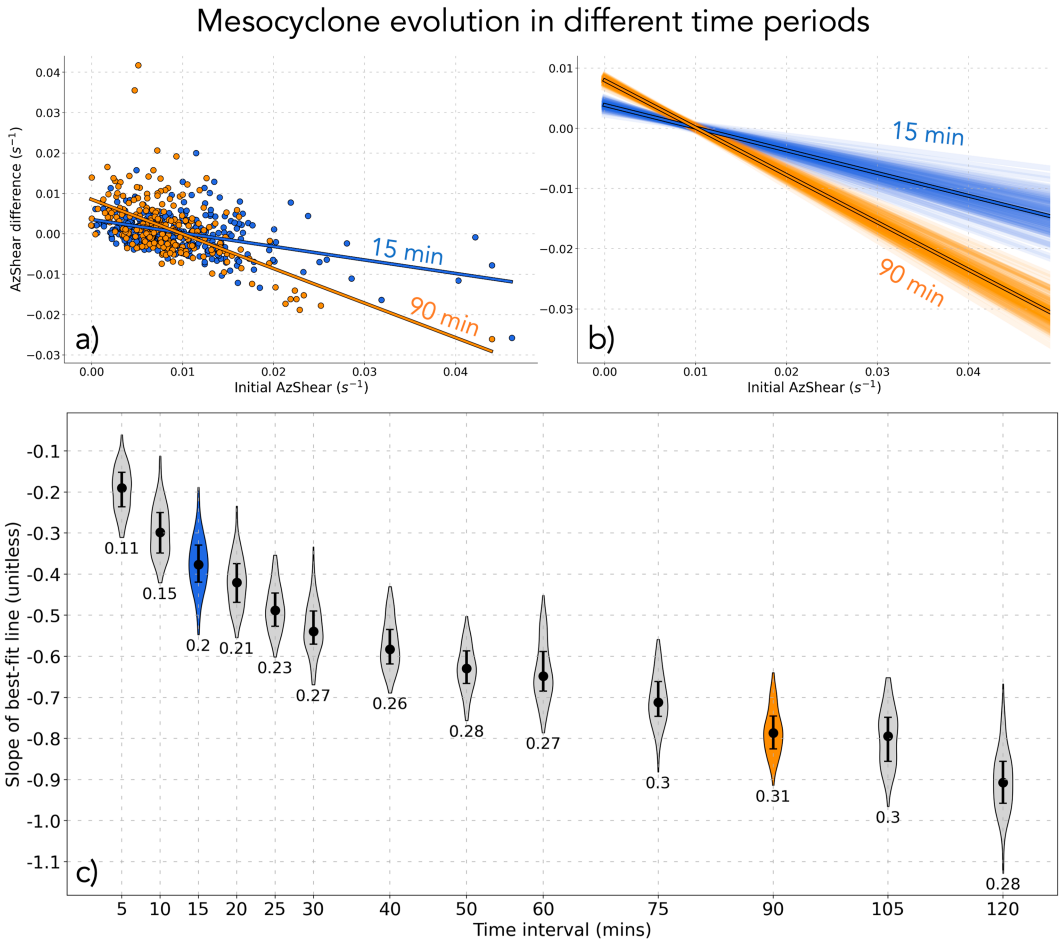

FIG. 1. (a) Scatterplot of the change in AzShear during 15-min (blue) and 90-min (orange) periods as a function of the initial AzShear at the start of the periods. The periods were randomly selected across all $n = 342$ supercell life cycles, and the sample size grows smaller as the time interval gets larger (due to the length of available supercell tracks; $n = 326$ and $n = 236$ for the 15- and 90-min periods, respectively). The linear least squares regression for each distribution is shown. (b) As in (a), but showing the regressions for 100 iterations of randomly selected 15-min (blue) and 90-min (orange) periods across all available supercell life cycles. Some differences between (b) and (a) were made for clarity: The *y*-axis limits are different, scatter points are removed, and the regression lines are widened and slightly transparent. The two thicker lines, outlined in black, are plotted using the median slope and median *x* intercept for each distribution of $n = 100$ linear least squares regressions. (c) Finally, the 100 slopes each from the two distributions of regressions in (b) are represented as violin plots (blue and orange violins at 15 and 90 min, respectively). Violins representing the distribution of $n = 100$ regression slopes for other time intervals ranging from 5 to 120 min are shown in gray. The interquartile range of each distribution is shown, along with the median (black dot). Median R^2 values for each distribution are plotted beneath each violin. The smallest sample size is $n = 142$ supercells for the 120-min time interval.

To test how sensitive the regressions might be to the different portions of the supercell life cycles that were selected, we repeated the regression $n = 100$ times for randomly selected time periods that were either 15 or 90 min long. The resulting regressions are plotted in Fig. 1b, and the median regression is highlighted. Despite which 15- or 90-min periods are randomly selected, the magnitudes of the slopes of the regressions are very consistently greater for 90-min periods than 15-min ones. Finally, the 100 individual slopes from the two distributions of regressions—ranging from around −0.2 to −0.9—comprise the colored violin plots in Fig. 1c. The violins at other time intervals represent the same distribution of slopes calculated for different time intervals ranging from 5 to 120 min.[1]

[1] The range of sample sizes ranges from 326 (for the 5-min time interval) to 142 (for the 120-min time interval). The number of supercells steadily decreases as the time interval increases because some supercells were sampled for shorter periods than others; in the F22 dataset, this was due to 1) a shorter-lived supercell within 75 km of the nearest WSR-88D location and/or 2) faster storm motion yielding less radar volumes within the 75-km-radius analysis window. For the statistics presented here, this range of sample sizes yields meaningful relationships at all time intervals.

Across all time intervals, the slopes of the regressions are negative, and a positive x intercept exists (around 0.01 s^{-1}, discussed more later). The regression slopes steadily decrease (increase in magnitude) from around −0.2 to −0.5 from 5- to 30-min intervals and then decrease more gradually thereafter to around −0.9 at the 120-min interval. All medians of adjacently plotted violins are significantly different at the 99% confidence level,[2] except for the 50–60- and 90–105-min intervals. This yields high confidence that the tendency for stronger mesocyclones to weaken and weaker mesocyclones to strengthen is increasingly impactful at longer time scales.

For smaller time periods (e.g., 5–30 min), a weaker relationship between initial AzShear and short-term AzShear variations is consistent with many other factors influencing short-term fluctuations in mesocyclone intensity (e.g., environmental inhomogeneities like cell mergers, fronts, outflow boundaries, and terrain). This further motivates our subsequent analysis of the impact of cell mergers on mesocyclone evolution. However, even these weaker relationships are statistically significant. Median p values at each time interval—within each $n = 100$ distribution of regressions—are negligible when using the Wald test;[3] confidence at the 99% level is reported for nearly all median regression slopes shown in the violins in Fig. 1c, except for some regressions in the 5- and 10-min time intervals featuring p values between 0.05 and 0.1, indicating 90%–95% confidence. For larger time intervals (e.g., 60–120 min), stronger relationships exist between initial AzShear and longer-term AzShear variations. Over periods of around 1 h and longer, the magnitudes of the regression slopes gradually increase, and over 25% of the mesocyclone's change in intensity is explained by the mesocyclone's initial intensity (see the median R^2 values > 0.25 beneath each violin at time intervals ≥ 30 min).

If weaker mesocyclones tend to strengthen and stronger mesocyclones tend to weaken, is there some sort of value that may distinguish "weaker" versus "stronger"? The x intercepts around 0.01 s^{-1} in Figs. 1a and 1b and Figs. 2–4 in F23 are a crude first guess at what such a value might be. This finding supports the vertical vorticity threshold traditionally used for identifying mature mesocyclonic rotation in simulations and observations (e.g., Moller et al. 1994). Based on F23, mesocyclones with initial AzShear < 0.01 s^{-1} tend to strengthen during the next 30 min and vice versa for those with initial AzShear > 0.01 s^{-1}. Interestingly, the AzShear values for the same analysis shown in F23—but for time intervals ranging from 5 to 120 min—are roughly around 0.01 s^{-1} (i.e., the x intercepts in Figs. 1a,b). A similar AzShear value is shown in Fig. 2 (i.e., initial AzShear = 0.008–0.01 s^{-1} where $y = 50\%$),

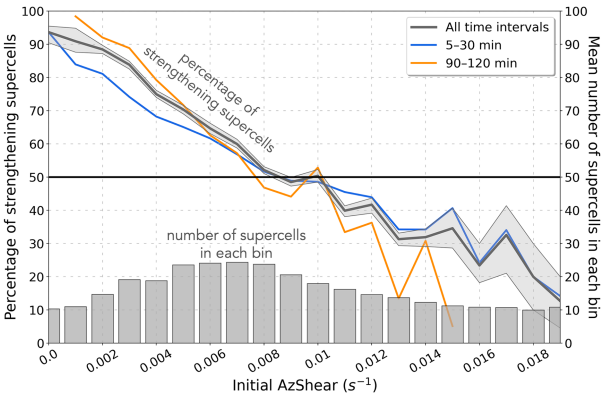

FIG. 2. Distribution of the percentage of mesocyclones that strengthened (left y axis) during any subsequent time period (gray; 5–120 min) binned by initial mesocyclone AzShear. The bins range from 0 to 0.018 s^{-1} every 0.001 s^{-1}. The gray bins represent the mean number of samples in each bin across all time intervals (right y axis); only bins with mean sample sizes greater than 10 were retained. Each bin represents a range of 0.001 s^{-1} AzShear, and the x coordinate for the data point for each bin is plotted at the starting point of the bin; e.g., the percentage for the initial AzShear bin from 0.005 to 0.006 s^{-1} is plotted at $x = 0.005$ s^{-1}. The distribution of percentages of strengthening vs weakening mesocyclones at each bin was computed across all time intervals (5–120 min) for all randomly selected periods ($n = 100$, as in Fig. 1). The thick, dark gray line represents the mean of each distribution ($n = 100$) for each bin, and the shading represents the interquartile range. The blue and orange lines are similar to the dark gray line, except they show the percentage of strengthening supercells over a subset of subsequent time intervals: Blue represents 5–30-min intervals, and orange represents 90–120-min ones. For clarity, the interquartile ranges (e.g., shading) and mean sample sizes in each bin (e.g., the vertical bars) are not shown for these subsets.

which shows the percentages of mesocyclones, binned by their initial AzShear value, that strengthened during any subsequent time interval (e.g., averaged over all time intervals from 5 to 120 min).

Across the parameter space of initial AzShear values—ranging from around 0 to 0.019 s^{-1}—a value around 0.01 s^{-1} appears to be a loose threshold between mesocyclones that are more likely to strengthen versus weaken during any subsequent time interval. This is when the percentage of strengthening supercells crosses the 50% threshold, trending toward more strengthening mesocyclones in one direction of initial AzShear and more weakening ones in the other. Consistent with the analysis in Fig. 1, the signal for weaker supercells to strengthen (and vice versa) is slightly stronger over longer time periods (e.g., 90–120 min) rather than shorter ones (e.g., 5–30 min). This is seen by comparing the slopes of the orange and blue lines in Fig. 2. Also, despite smaller mean sample sizes in both tails of the initial AzShear spectrum (e.g., <0.002 and >0.014 s^{-1}), the range of the percentage of strengthening mesocyclones is much smaller for smaller initial AzShear values. In other words, the interquartile range is smaller for smaller initial AzShear than for larger initial AzShear. The high confidence in initially weaker mesocyclones strengthening is strongly influenced by the analysis technique, which did not

[2] This was found using $n = 10\,000$ Monte Carlo simulations to test the difference in medians of two $n = 100$ distributions of regression slopes (e.g., two violins from Fig. 1c) against the resulting histogram comprising 10 000 simulated median differences.

[3] This is the default for the linear regression computation using scipy.stats.linregress. The null hypothesis for this test is that the slope of the regression is zero, and the test assumes normally distributed input. This is appropriate for the AzShear differences across all time intervals (not shown).

consider any mesocyclones that dissipated during the subsequent time period; this is further discussed below.

A key caveat to this analysis is that all mesocyclones persisted for the entirety of the time intervals analyzed. For example, roughly 95% of mesocyclones with initial AzShear from 0 to 0.001 s^{-1} strengthened, but this percentage is only derived from time intervals during each supercell's life cycle; in other words, if the starting point of a 30-min period was randomly selected for a supercell with an initial AzShear of 0.0005 s^{-1} and that supercell's time series ended 15 min later, an alternate time period during the supercell's life cycle was examined. Thus, the percentages in Fig. 2 are conditional probabilities: The condition is the persistence of the mesocyclone during the desired time interval. This caveat, however, does not influence the signal for initially strong mesocyclones to subsequently weaken. In other words, strong mesocyclones are not generally steady state but rather exhibit large short-term fluctuations in intensity.

The analysis thus far supports the idea that mature supercell mesocyclones generally regress toward some mean intensity. As the analyzed time period increases (e.g., from 5–30 to 90–120 min), the magnitude of this inverse relationship increases (e.g., Figs. 1 and 2), assuming that the mesocyclone persists for the entire period. This signal exists in all phases of storm life cycles in this sample of tornadic and significant-severe supercells. Across these supercells in the F22 dataset, the mean intensity is characterized by an AzShear value of around 0.01 s^{-1}. Given observed x intercepts around 0.012 s^{-1} in a more volatile environment (e.g., 27 April 2011; Fig. 4 in F23), although this is just one case, we hypothesize that this mean intensity is at least somewhat influenced by the background environment. This idea is also supported by the wealth of prior work relating characteristics of the background environment to the intensity of supercell hazards. The subsequent analysis offers the first quantification of this relationship.

4. Environmental influences on low-level mesocyclone strength

a. *Links between mesocyclone intensity and simultaneous environmental conditions*

We tested a variety of SFCOA kinematic and thermodynamic parameters including CAPE, CIN, LCL, bulk wind difference (BWD; 0–1, 0–3, and 0–6 km), and SRH (0–1 and 0–3 km). Mixed-layer (ML; lowest 100 hPa), surface-based (SB), and most-unstable (MU) parcels were used for separate calculations of CAPE, CIN, and LCL. Each of these variables was linearly regressed against different percentiles (25th, 50th, 75th, 90th, 95th, and 98th) of AzShear (computed using the entire time series) for each storm. The goal was to test various percentiles across AzShear intensity (e.g., 25th, 50th, and 75th percentiles) and focus on the upper end of the parameter space (e.g., 90th–98th percentiles). We limited the analysis to storms that persisted for at least 10 volume scans (roughly 50 mins) to increase confidence in the representativeness of each percentile. Once each percentile for each storm was found, all times that the mesocyclone AzShear met or exceeded that percentile were compiled, and the mean time was computed and paired with the closest hourly SFCOA variables. During the 2005–11 period (containing higher-vertical-resolution RUC analyses), this yielded a sample size of 223 mesocyclones (differing from the larger sample sizes presented previously which included 2003–04). We documented the p and R^2 values for each regression (Fig. 3) and used these to inform statistical significance as described below.

Across all percentiles of AzShear intensity, the most strongly correlated environmental parameter is 0–3-km SRH (Figs. 3 and 4a). The magnitude of the correlation peaks at the 95th percentile of AzShear with $p = 0$ and $R^2 = 0.3131$. This suggests that almost one-third of the variability in the 95th percentile of AzShear (a measure of the "peak intensity") is explained by variability in environmental 0–3-km SRH. This relationship is consistent with previous observational (e.g., Rasmussen and Blanchard 1998; Thompson et al. 2003; Craven and Brooks 2004; Coniglio and Parker 2020), numerical (e.g., Markowski and Richardson 2014; Coffer and Parker 2017; Dahl 2017; Flournoy et al. 2020; Goldacker and Parker 2021; Coffer et al. 2023), and theoretical (e.g., Davies-Jones 1984, 2002; Peters et al. 2019) studies finding that greater SRH yields a stronger low-level mesocyclone. The linkage is driven by barotropic processes (e.g., tilting and vertical stretching of initially horizontal vorticity) from as low as a few hundred meters AGL (Coffer et al. 2023) up through the low levels of interest (3 km AGL, e.g., Davies-Jones 1984).

The 0–1-km SRH is also modestly correlated with maximum 0–3-km AzShear across all percentiles. The respective R^2 values for these regressions peak at the upper end of the AzShear percentile range ($R^2 = 0.2755$ at the 95th percentile). Across all percentiles, changes in low-level SRH (0–1 and 0–3 km) explain roughly 19%–31% of the variability in peak AzShear. The 0–1-km SRH (and perhaps lower layers) might exhibit a stronger correlation with peak AzShear values if lower-level mesocyclone rotation was examined (e.g., 1 km AGL) rather than the 0–3-km maximum AzShear used here. Similar, generally slightly weaker relationships exist between peak AzShear percentiles and various layers of bulk shear (including the 0–1-, 0–3-, and 0–6-km layers). The greatest correlation between these shear layers and peak AzShear intensity is for 0–3-km BWD at the 95th and 98th percentiles (Figs. 3 and 4b). The slopes of the regressions are significant across all shear layers and AzShear percentiles ($p = 0$ in all cases) and explain around 10%–27% of the variability in peak AzShear. Like SRH, R^2 values for these regressions peak in the upper end of the AzShear distribution (at the 95th or 98th percentiles for all three layers of shear).

Thermodynamic parameters exhibited much less correlation with the AzShear percentiles than SRH and BWD. Of the thermodynamic parameters tested, LCL featured the strongest correlation. Between SB and MLLCLs, SBLCL exhibited the largest R^2, peaking at the 98th percentile of AzShear with $p = 0.0003$ and $R^2 = 0.0616$ (Fig. 3). However, we focus on the regression between MLLCL and the 95th percentile of AzShear, because it contains the second-largest R^2 value of any of the LCL-related regressions ($R^2 = 0.0569$), and it is the greater of the two for the 95th AzShear percentile

Statistics of linear-least squares regressions between environmental variables and different AzShear percentiles

	25th percentile AzShear		50th		75th		90th		95th		98th	
	p	R^2	p	R^2	p	R^2	p	R^2	p	R^2	p	R^2
MLCAPE	0.9976	0	0.9413	0	0.5078	0.0019	0.944	0	0.7526	0.0005	0.7899	0.0003
SBCAPE	0.6668	0.0008	0.3478	0.0038	0.6339	0.001	0.4039	0.0031	0.3857	0.0034	0.5768	0.0015
MUCAPE	0.9021	0.0001	0.8639	0.0001	0.7272	0.0005	0.7595	0.0004	0.8963	0.0001	0.9663	0
MLCIN	0.6116	0.001	0.8845	0.0001	0.7979	0.0003	0.2438	0.0061	0.4362	0.0028	0.2915	0.0053
SBCIN	0.7431	0.0005	0.5475	0.0016	0.5477	0.0016	0.9235	0	0.6112	0.0012	0.552	0.0017
MUCIN	0.9677	0	0.8653	0.0001	0.7506	0.0004	0.6303	0.001	0.6819	0.0008	0.8523	0.0002
MLLCL	0.0664	0.0146	**0.0054**	**0.0332**	**0.0032**	**0.0371**	**0.0009**	**0.0477**	**0.0003**	**0.0569**	**0.002**	**0.0439**
SBLCL	**0.0064**	**0.0324**	**0.0013**	**0.0451**	**0.002**	**0.0413**	**0.0004**	**0.0554**	**0.0005**	**0.0548**	**0.0003**	**0.0616**
SHR01	**0**	**0.1769**	**0**	**0.226**	**0**	**0.2352**	**0**	**0.2266**	**0**	**0.2363**	**0**	**0.2305**
SHR03	**0**	**0.1645**	**0**	**0.2068**	**0**	**0.2282**	**0**	**0.248**	**0**	**0.2659**	**0**	**0.2659**
SHR06	**0**	**0.1034**	**0**	**0.1295**	**0**	**0.1653**	**0**	**0.2046**	**0**	**0.2279**	**0**	**0.2028**
SRH01	**0**	**0.1877**	**0**	**0.2436**	**0**	**0.2488**	**0**	**0.2472**	**0**	**0.2755**	**0**	**0.2708**
SRH03	**0**	**0.208**	**0**	**0.2581**	**0**	**0.2723**	**0**	**0.2842**	**0**	**0.3131**	**0**	**0.305**
SCP	**0**	**0.1435**	**0**	**0.1824**	**0**	**0.2356**	**0**	**0.2041**	**0**	**0.2429**	**0**	**0.2124**

R^2 increases at 1-h lag by > 0.05 | R^2 increases at 1-h lag by 0–0.05 | R^2 decreases at 1-h lag by 0–0.05 | R^2 decreases at 1-h lag by > 0.05

R^2 is greater with 1-h time lag ← → R^2 is greater with no time lag

FIG. 3. Table showing p and R^2 values from Wald tests of the various linear least squares regressions described in the text. These statistics are for simultaneous regressions computed between peak AzShear thresholds and environmental variables extracted as close to the mean time period of the AzShear values as possible. The columns represent different percentiles of AzShear (25th–98th), and each row contains statistics for a particular environmental variable. A thin line separates thermodynamic and kinematic/composite variables. Bold cells contain regressions that are statistically significant at the 95% confidence level ($p < 0.05$). Shading indicates the difference between the values shown here and those computed from 1-h time-lagged regressions (i.e., the environmental variables were extracted roughly 1 h before the mean AzShear time period). Green shading indicates that the R^2 values for the simultaneous regressions (shown here) are greater than the time-lagged ones and vice versa for brown shading. There are two instances where the simultaneous regression was significant but the 1-h time-lagged regression was not; these cells are not shaded.

in which 0–3-km SRH exhibits the greatest R^2 value. At this percentile, roughly 6% of the variability in "peak" AzShear is explained by changes in environmental MLLCL. This is about one-fifth of the percent of peak AzShear explained by SRH variability. We revisit the linkage between MLLCL and peak AzShear in the discussion section.

The strongest relationships between the 95th percentile of AzShear and kinematic and thermodynamic parameters were with 0–3-km SRH and MLLCL, respectively. Figure 5a shows the 95th percentile of AzShear plotted in this phase space. Figure 5b shows the same scatterplot binned by intervals of 0–3-km SRH (every 100 $m^2 s^{-2}$) and MLLCL (every 250 m). The tendency for the 95th percentile of (or peak) AzShear to increase as 0–3-km SRH increases and as MLLCL decreases is clear. Even when only considering the binned means with larger contributing sample sizes (e.g., >5 mesocyclones), the 95th percentile of AzShear steadily increases from around 0.015 to 0.025 s^{-1} as 0–3-km SRH increases and MLLCL decreases. Consistent with the relative signals in Fig. 4, peak AzShear increases more rapidly as 0–3-km SRH increases than as MLLCL decreases.

Given the strength of the regression between peak AzShear and the low-level environmental shear profile—especially related to 0–3-km SRH and BWD (Figs. 4a,b)—we investigated how sensitive peak low-level mesocyclone strength may also be to the concentration of shear in lower levels versus midlevels. To examine this, we compared the 0–3-km BWD to the ratio of 0–3- to 0–6-km BWD. Plotting these parameters against each other (Fig. 6) shows how concentrated shear magnitudes are in low- versus midlevels and whether this may be associated with differences in peak AzShear. The clearest trend in Fig. 6 is for peak AzShear to generally increase as 0–3-km BWD increases (consistent with Fig. 4b). There also seems to be a slight tendency for peak AzShear to increase as the ratio of 0–3- to 0–6-km BWD decreases (e.g., peak AzShear increases in the negative-y direction). In other words, as 0–3-km BWD remains fairly constant, increasing midlevel shear is associated with a slightly stronger low-level mesocyclone. Because very little of the 3–6-km layer, if any, contributes to the effective inflow layer, this weak relationship could be more associated with shear-influenced precipitation fallout patterns (Warren et al. 2017) and/or vertical accelerations (Parker 2017; Muehr et al. 2024) that then may influence low-level mesocyclone strength.

Due to the prevalence of 0–6-km BWD and mixed-layer convective available potential energy (MLCAPE) in the severe-weather forecasting and climate (e.g., Brooks 2013; Púčik et al. 2017; Taszarek et al. 2021) literature, we also show how the 95th percentile of AzShear varies across this parameter space (Fig. 7). The 0–6-km BWD exhibited a significant correlation with all percentiles of AzShear; the maximum is for the 95th percentile with $p = 0$ and $R^2 = 0.2028$. MLCAPE exhibited no significant correlation with any percentile of AzShear. There is perhaps a slight trend for peak AzShear to increase toward the upper-right corner of the plot. However, this trend is not as evident when examining binned means and is driven almost solely

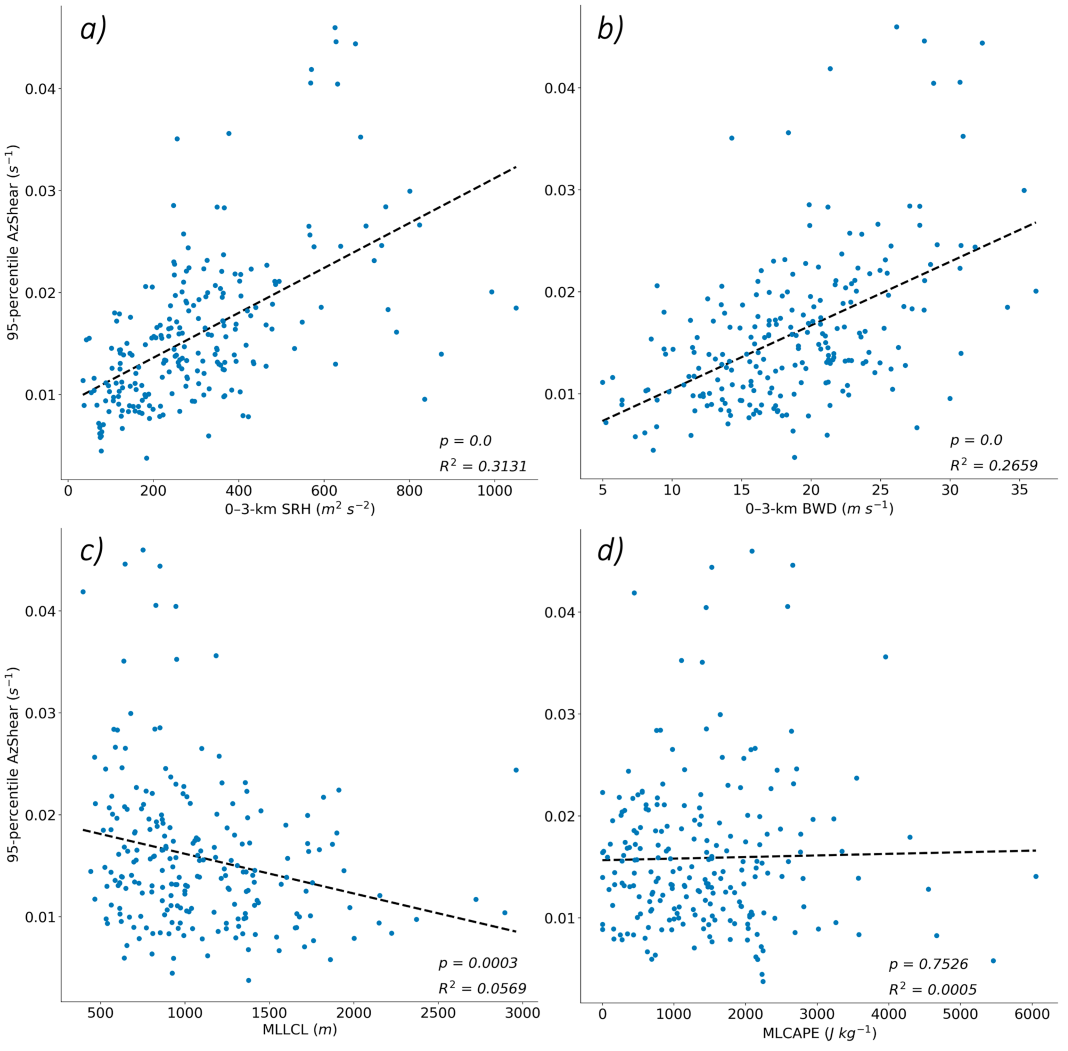

FIG. 4. Scatterplots of select environmental parameters linearly regressed against the 95th percentile of AzShear for $n = 223$ mesocyclones. The R^2 and p values for each regression are shown in the bottom-right corner of each panel.

by the positive relationship between peak AzShear and 0–6-km BWD. Across the parameter space occupied by binned means with a larger sample size (e.g., >5 mesocyclones), the 95th percentile of AzShear steadily increases from 0.010–0.015 s^{-1} to nearly 0.030 s^{-1}, mostly as 0–6-km BWD increases.

b. *Links between mesocyclone intensity and time-lagged environmental conditions*

Acknowledging the significant relationships between mesocyclone intensity and environmental conditions at roughly the same time, we wondered how strongly mesocyclone intensity may be related to previous environmental conditions. Could a mesocyclone's intensity be strongly related to environmental conditions 1 h prior, or perhaps as far back as at the time of convection initiation? The shading in Fig. 3 reveals some aspects of these time scales. For the higher AzShear percentiles (95th and 98th, the primary focus of this paper), R^2 values are larger for the "simultaneous" regressions (i.e., those computed between the mean time period that the mesocyclone exhibited AzShear above the designated percentile and the closest hourly environmental fields) than the "1-h time-lagged" regressions (i.e., those computed between the mean time period that the mesocyclone exhibited AzShear above the designated percentile and the environmental fields roughly 1 h prior). The opposite is true at lower percentiles of AzShear (e.g., 25th–90th). The same trends are generally observed when comparing the simultaneous regressions with the "convection initiation" regressions (i.e., the same as above except using the environmental fields closest to the beginning of each storm's life cycle). This suggests that while a measure of the mature, baseline mesocyclone intensity (e.g., around the 50th percentile of AzShear) may be more closely tied to historical environmental conditions, the most intense periods of a mesocyclone's life cycle may be more related to shorter-term environmental changes (e.g., within the most recent 30 min based on this analysis).

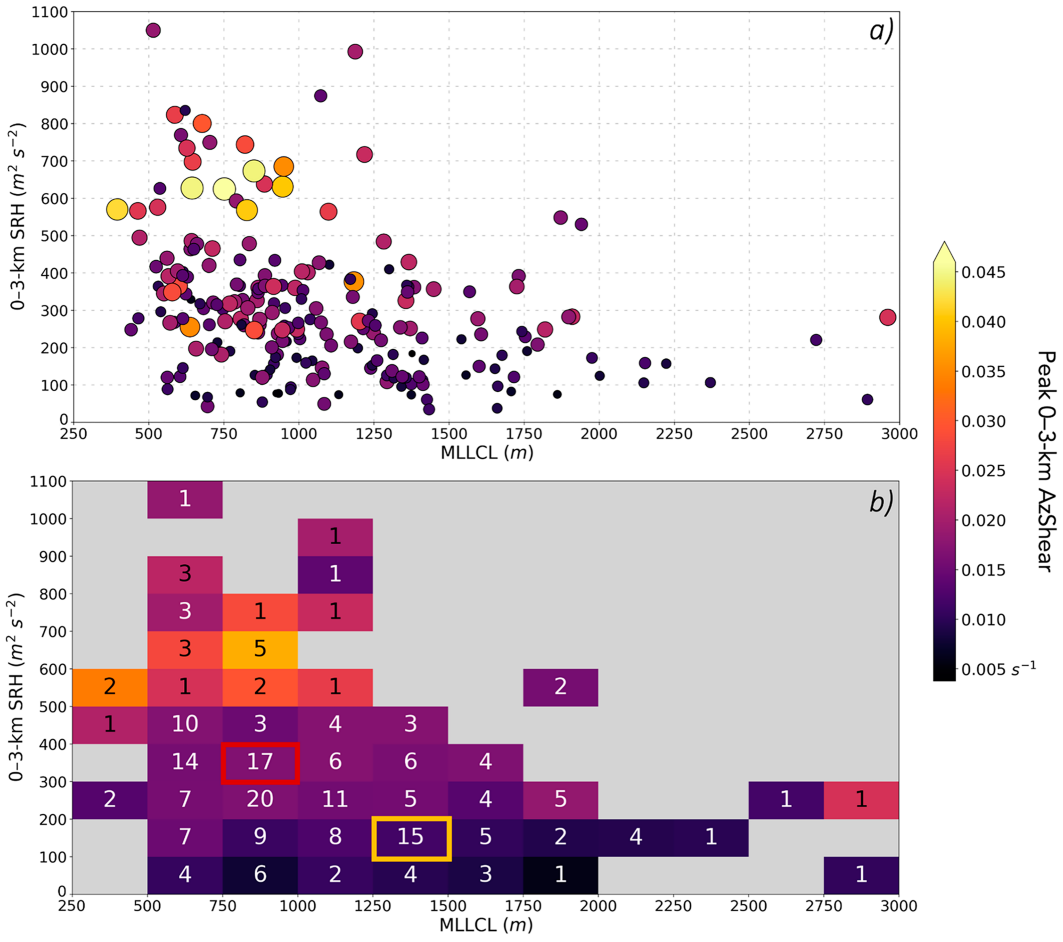

FIG. 5. (a) Scatterplot of the 95th percentile of AzShear in a MLLCL–SRH phase space for the $n = 223$ mesocyclones (e.g., the same mesocyclones plotted in Fig. 3). Dot colors represent the 95th percentile of AzShear, and the size of each dot is proportional to the magnitude of the 95th percentile of AzShear (i.e., larger dots indicate a greater magnitude). (b) Means of the AzShear values in (a) binned by MLLCL and 0–3-km SRH. The background color of each bin represents the mean 95th percentile of AzShear within that bin. The color bar corresponds to both panels. The number in each bin is the number of points contributing to each mean calculation. Gray areas indicate bins with no observations. The bins outlined in red and yellow are referenced in the discussion section and Fig. 10.

This motivated further analysis of temporal environmental evolution (e.g., like those documented in Davenport 2021) and its possible relation to mesocyclone intensity. We first examined the changes in AzShear during random 1-h periods of supercell life cycles and regressed them against environmental changes at the same time (to the nearest hour). We also performed the same regressions but for environmental changes during the previous hour (e.g., the 1-h period comprising the roughly 1–2-h period before the AzShear analysis time frame). The hourly changes in AzShear were computed by subtracting the mean AzShear at the start of the period from the mean AzShear at the end of the period; the roughly 10-min mean values were found by averaging the AzShear value at the start of the random 1-h period and the AzShear values just before and just after (spanning a roughly 10-min time period). The environmental changes were computed using simple subtractions of the hourly SFCOA fields. We found no significant relationships ($p < 0.05$) between AzShear changes and any of the environmental variables that we tested (i.e., those listed in Fig. 3; not shown). In other words, for example, we did not see an association between 1-h increases in 0–3-km SRH and a strengthening low-level mesocyclone during that same time frame or during the following 1-h period across random periods of supercell life cycles. This probably warrants further investigation given known biases in the SFCOA and RUC fields (e.g., underestimating low-level storm-relative winds and wind shear; Coniglio and Jewell 2022) and the possibility that any associations operate on smaller spatiotemporal scales (i.e., not resolvable on an hourly, 40-km horizontal grid).

There are somewhat clearer trends when, instead of assessing random periods, we examine AzShear and environmental variability leading up to periods of peak (i.e., 95th percentile) AzShear. Figure 8 shows these trends for 0–3-km SRH and MLLCL, which both exhibited significant relationships with

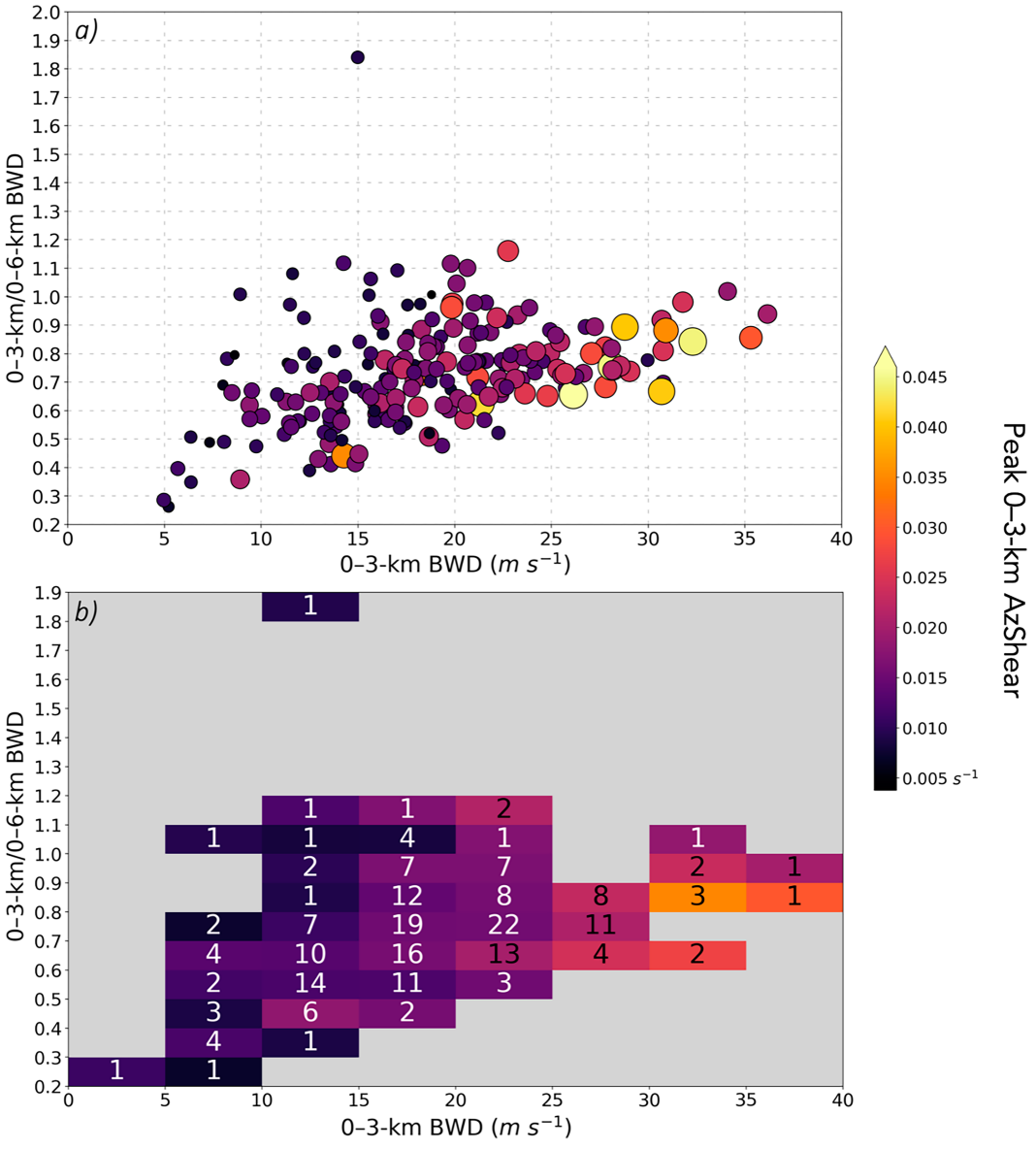

FIG. 6. As in Fig. 5, but for the 0–3-km BWD and ratio of 0–3- to 0–6-km BWD phase space.

peak AzShear (Figs. 4 and 5). The sample sizes for the simultaneous and 1-h time lag distributions are $n = 67$ and 15, respectively.[4] Fig. 8a shows that hourly increases in 0–3-km SRH are more often associated with increasing AzShear, both during roughly the same time frame (i.e., simultaneous) and 1 h after the environmental 0–3-km SRH increase (i.e., 1-h time lag). The 1-h trends in MLLCL are also relatively well distributed about $x = 0$ (Fig. 8b); although the signal is not quite as strong as that for 0–3-km SRH, much of the interquartile ranges of the distributions of MLLCL variation lie to the left of $x = 0$. This suggests that decreasing MLLCL is more often associated with increasing AzShear and vice versa for increasing MLLCL.

The same box-and-whisker plots for all of the variables tested are shown on the right-hand side of Fig. 8 (the MLLCL and 0–3-km SRH distributions that are shown in Figs. 8a and 8b are outlined in yellow and purple, respectively). In general, the box-and-whisker plots do not reveal any large, meaningful differences between the simultaneous and 1-h time lag distributions.

[4] This is because the samples were limited to storms that met the following criteria: 1) SFCOA data were available (e.g., excluding storms in 2003–04); 2) two or more AzShear values exceeded the 95th percentile of AzShear; 3) these points occurred within a 30-min window (i.e., to isolate one individual, intense-mesocyclone period from each storm rather than possibly averaging over multiple); and 4) that 30-min period occurred at least 1 h (for the simultaneous sample) or 2 h (for the 1-h time lag sample) after the start of each storm's time series. The fourth criterion was necessary for ensuring adequate environmental sampling in advance of the peak AzShear period.

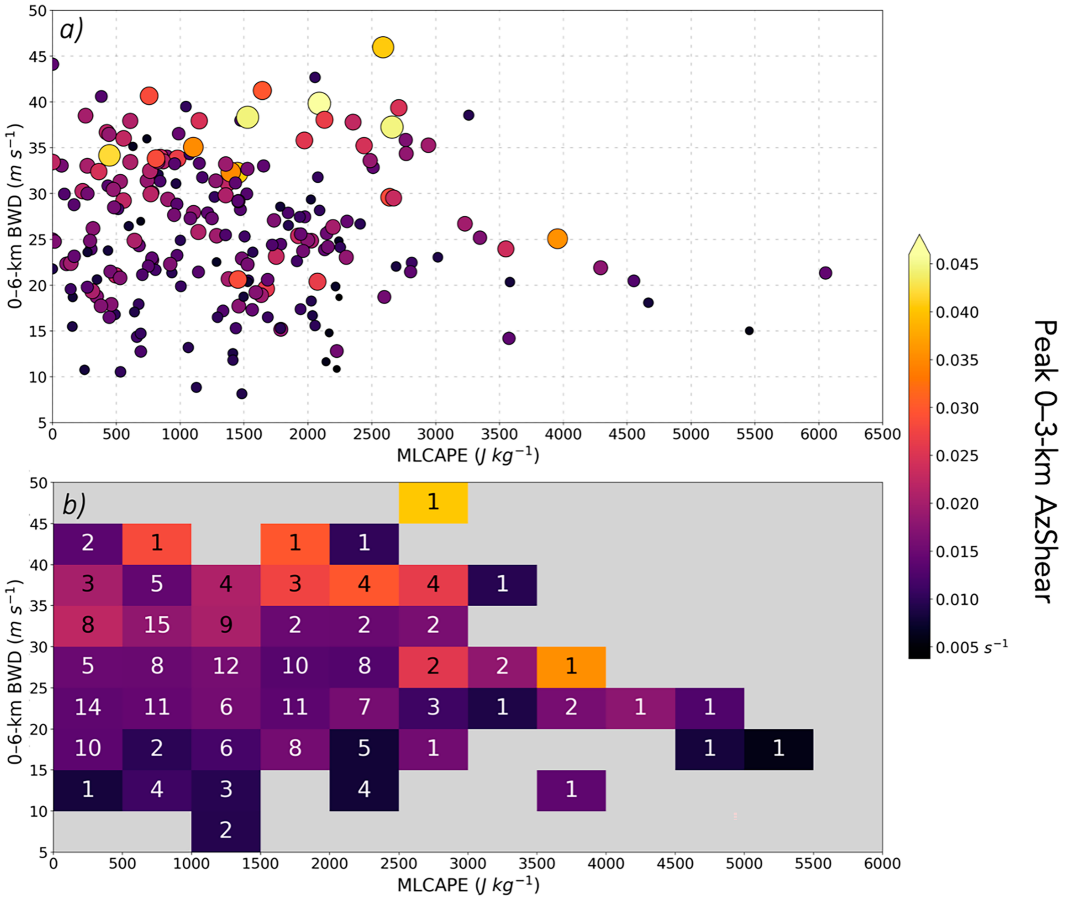

FIG. 7. As in Fig. 5, but for the MLCAPE and 0–6-km BWD phase space.

If anything, increasing 0–3-km SRH (Fig. 8a) may be more strongly associated with increasing AzShear during the subsequent hour as opposed to during roughly the same time period (e.g., comparing the blue and orange box-and-whisker plots along the x axis in Fig. 8a). A similar signal exists for SCP and SHR06 (0–6 km AGL shear); general increases in both parameters are observed in the 1-h period preceding peak AzShear, but the trend distributions are more negligible during the peak AzShear period itself. Also, mesocyclones at peak intensity tend to be associated with relatively constant CAPE (or even increasing when looking at MLCAPE) in the 1-h period preceding peak AzShear, but generally decreasing CAPE during the peak AzShear period. This is consistent with the idea that mesocyclones take time to respond to environmental changes, and their intensity is thus not only a function of environmental characteristics at that time but also leading up to that time (Davenport 2021). The thermodynamic signal is also consistent with the observed relationships between peak mesocyclone maturity and the diurnal cycle (e.g., Coffer and Parker 2015; Gropp and Davenport 2018; Davenport 2021). In this dataset, it seems like low-level mesocyclone intensity may be meaningfully influenced by temporal trends in 0–3-km SRH around 1–2 h prior. However, our confidence in this relationship is limited due to the dwindling sample sizes (i.e., $n = 15$ for the 1-h time lag distributions), which also preclude analysis of possible relationships between mesocyclone intensity and environmental trends earlier in the storms' life cycles (e.g., two or more hours in the past).

5. Merger influences on low-level mesocyclone strength

In light of recent findings showing that cell mergers do not generally influence mesocyclone intensity in a consistent way (F23), we assess the possibility that stronger relationships may exist in different environments. Of the 169 supercells in the F22 dataset that experienced cell merger events (out of 342 total), 126 contained 1) sufficient AzShear observations on either side of the merger event and 2) sufficient RUC vertical grid spacing (25 hPa, i.e., excluding events prior to 2005) to associate environmental characteristics with mesocyclone evolution. This sample size is smaller than previous samples because this portion of the analysis focuses on supercells that experienced cell mergers. We tested the same environmental parameters described in the previous section. Of all these parameters, the only one that exhibited a significant relationship with across-merger AzShear differences was MLLCL ($p = 0.0385$). The resulting scatterplot and least squares linear regression line are shown in Fig. 9a.

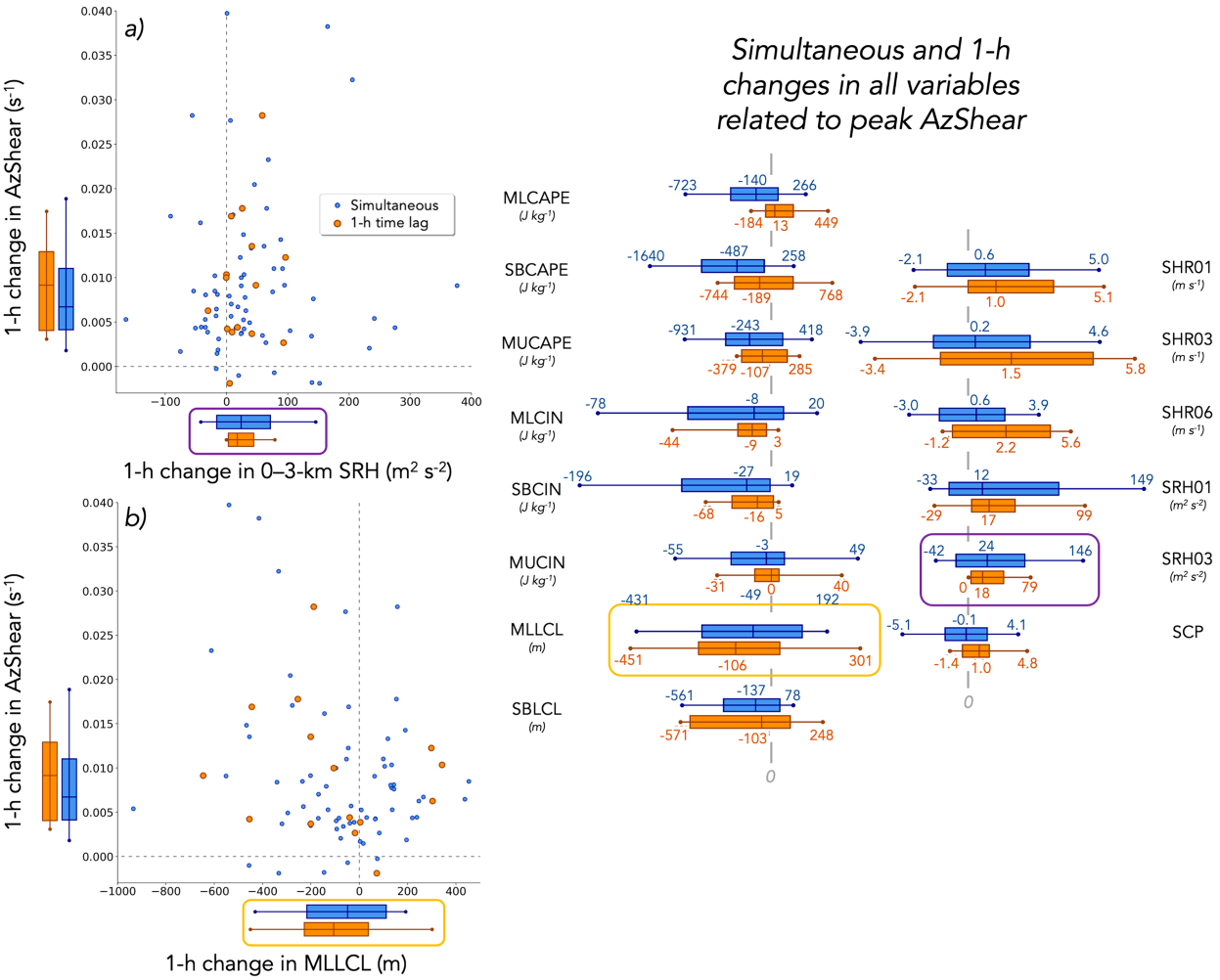

FIG. 8. (a) Scatterplot of the 1-h change in AzShear leading up to the time of peak AzShear vs the 1-h change in 0–3-km SRH for each storm. The time of peak AzShear was defined as the mean of all times within the 30-min period (or the first if there were multiple) in which the AzShear exceeded the 95th percentile for each storm. The blue dots represent simultaneous 0–3-km SRH changes; in other words, the end of the 1-h period was defined as the hourly SFCOA time that was closest to the time of peak AzShear (these times are anywhere from 0 to 30 min apart). The orange dots represent 1-h time-lagged 0–3-km SRH changes, in which the 1-h environmental period ended roughly 1 h (i.e., between 30 and 90 min) before the time of peak AzShear. The x and $y = 0$ axes are highlighted with gray dashed lines, and box-and-whisker plots represent the interquartile and 10th/90th percentiles of each distribution. (b) As in (a), but for MLLCL. The right panel shows box-and-whisker plots representing the same distributions as in (a) and (b) for all of the tested variables, including simultaneous changes (blue) and changes in the 1 h leading up to the peak AzShear period (orange). The variables are presented in the same order as in Fig. 3, with thermodynamic variables on the left and kinematic and/or composite parameters on the right. The yellow and purple boxes indicate the distributions for MLLCL and 0–3-km SRH, respectively, that are also shown in (a) and (b). Note that the horizontal extent of each distribution scales with the range of observed values for each variable. Median and 10th- and 90th-percentile values for each variable are plotted for reference.

However, does this trend differ from randomly selected periods of mesocyclone evolution? In other words, is this trend unique to cell merger periods, or is it relatively ubiquitous across all phases of supercell life cycles (cell merger or not)? To analyze this, we extracted random 30-min periods of each supercell in the full dataset from 2005 to 2011 ($n = 247$) and computed the corresponding p and R^2 values of the trend between AzShear differences and MLLCL during those periods. We repeated this process 100 times (e.g., producing the statistics in Fig. 9a each time), and the resulting distributions of p (blue; left) and R^2 (orange; right) values are shown in the half-violins in Fig. 8b. The observed p value during merger events is 0.0385 (Fig. 9a), which lies at the 0.73 percentile of the distribution of p values of the 100 random events (Fig. 9b). The corresponding R^2 value (0.0341; Fig. 9a) lies at the 99.55 percentile of the R^2 values (Fig. 9b). This suggests high confidence (i.e., >99%) that the observed positive relationship between MLLCL and subsequent AzShear evolution is statistically different during merger periods than random periods of supercell life cycles.

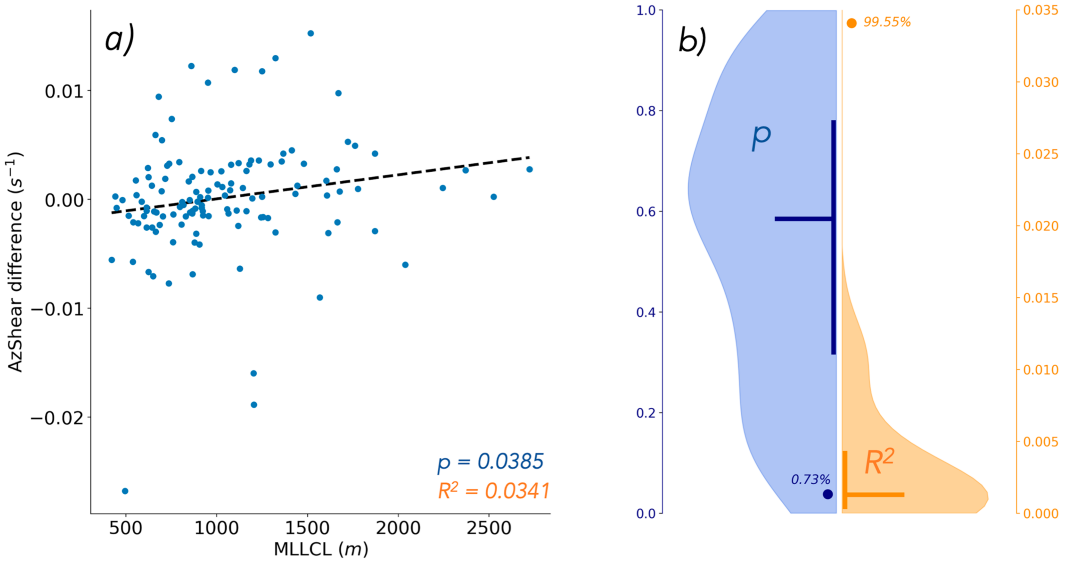

FIG. 9. (a) Scatterplots of MLLCL vs the difference in AzShear observed during $n = 126$ cell merger events. The p value—for a significance test whose null hypothesis is that the slope is zero—and the coefficient of determination R^2 are shown in the bottom-right corner. The linear least squares regression line is also shown. (b) Half-violin plots of p (left; blue) and R^2 (right; orange) values across $n = 100$ different iterations of the linear regression calculation between across-merger AzShear differences and environmental MLLCL [e.g., the line in (a)]. These calculations were completed for randomly selected 30-min periods of $n = 126$ supercell's life cycles. The axes are color coded with their respective violins (e.g., p on the left and R^2 on the right). The thick vertical lines represent the interquartile distributions, and the thick horizontal lines are the medians. The p and R^2 values for the AzShear–MLLCL relationship during cell merger events [i.e., shown in (a)] are plotted, along with the percent of the distribution in which they fall.

These findings suggest that a low-level mesocyclone's response to a cell merger may differ in environments with varying MLLCLs. As MLLCL increases, low-level mesocyclones are more likely to strengthen during a merger than weaken. While analyzing the physical processes responsible for this relationship is beyond the scope of this study, it is at least partially influenced by the significant, inverse relationship between premerger mesocyclone intensity and MLLCL (not explicitly shown but alluded to in Fig. 5). In other words, environments with higher MLLCLs are generally associated with weaker low-level mesocyclones. These might be expected to naturally strengthen during the subsequent 30-min period (e.g., F23). However, the p and R^2 values from Fig. 9 (during merger periods) lie in the upper and lower 1st percentiles (0.73% and 99.55%, respectively) of the statistical distributions during random supercell periods. This means that the generally weaker low-level mesocyclones residing in higher-MLLCL environments are more likely to strengthen during merger periods (as opposed to random periods) and vice versa for the generally stronger low-level mesocyclones residing in lower-MLLCL environments.

The relationship between MLLCL and across-merger AzShear differences is statistically significant at the 95% confidence level. However, the corresponding R^2 value is very small (0.0341) and suggests that variability in MLLCL is directly responsible for less than 4% of the mesocyclone's evolution. Thus, while the result may be statistically significant, it is not very operationally useful. This is consistent with recent and ongoing work showing that a mesocyclone's postmerger intensity can be strongly influenced by factors other than the background environment (e.g., Hastings and Richardson 2016; F22; LF23), including the mesocyclone-relative location of the merging cell, strength of the merging cell, and duration of the merger event. These factors are not captured here. We present the relationships between AzShear differences and MLLCL as the strongest of the parameters that we tested, with the applicability of the relationships thresholded by the limited observed variability in AzShear that they explain.

6. Discussion

The initial motivation for this analysis was to serve as a follow-up to recent studies examining the possible association of cell mergers with mesocyclone evolution. Given the findings of F22 and LF23 and the clarifications in F23, it is not surprising that no environmental parameter that we tested exhibits a strong correlation with across-merger differences in low-level mesocyclone intensity. The linear regression between across-merger AzShear and MLLCL featured a slope ($p = 0.0385$) and R^2 value (0.0341) that were significant with respect to the same values computed during random 30-min periods of supercell lifetimes. However, the very small R^2 value currently limits meaningful operational use. To this end, we did not find any significant and meaningful relationships between across-merger low-level mesocyclone evolution and hourly background environmental variables.

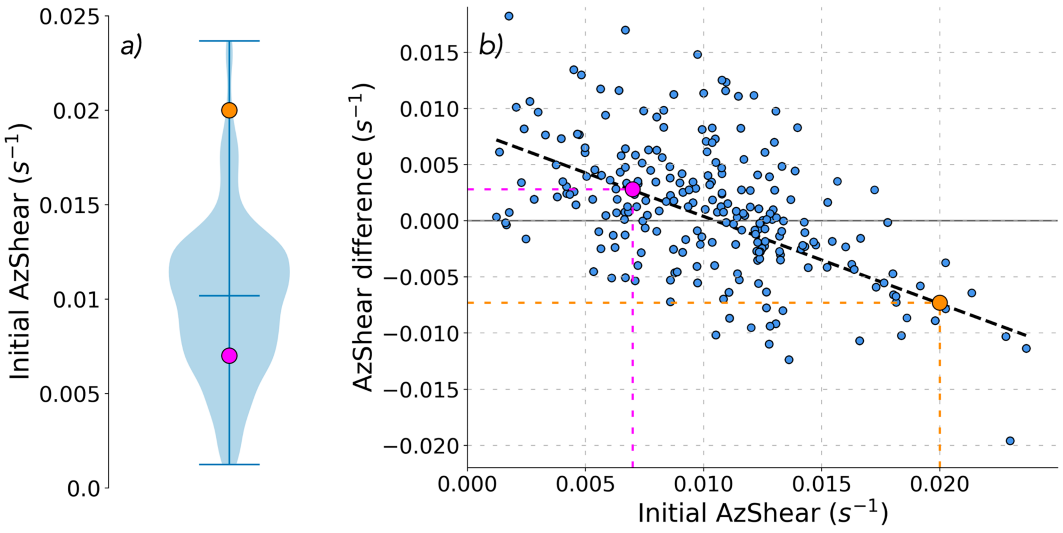

FIG. 10. (a) Violin plot showing the distribution of initial AzShear values for randomly selected 30-min periods of supercell life cycles within environments characterized by MLLCLs between 750–1000 m and 0–3-km SRH between 300 and 400 m^2 s^{-2}. The magenta and orange markers indicate hypothetical initial AzShear values of 0.007 and 0.02 s^{-1}, respectively, which are discussed in the text. (b) Scatterplot showing the initial AzShear and the subsequent 30-min AzShear difference for the same random periods in (a). The linear least squares regression line is shown as a dashed black line ($p = 0$ and $R^2 = 0.2966$), and the magenta and orange markers indicate points along the regression line where $x = 0.007$ and 0.02 s^{-1}.

Of the thermodynamic variables that we tested, MLLCL exhibited the strongest correlation with peak AzShear ($p = 0.0003$, $R^2 = 0.0569$; Fig. 4c). The scatter points in Fig. 4c occupy a meaningful portion of the MLLCL parameter space (e.g., around 500–2000 m AGL), in which the regression line exhibits a decrease in peak AzShear from around 0.019 to around 0.012 s^{-1}. In other words, lower-MLLCL environments may support higher tornado potential due to the presence of both 1) more buoyant surface outflow and 2) a stronger low-level mesocyclone. Although their analysis focused more on the alignment of near-surface circulations and those farther aloft, an inverse relationship between MLLCL and peak mesocyclone intensity was also noted in the simulations presented in Brown and Nowotarski (2019; e.g., their Fig. 7). In terms of tornado prediction, this may complement a number of studies that suggest that the inverse relationship between MLLCL and tornado production (e.g., Rasmussen and Blanchard 1998; Thompson et al. 2003; Craven and Brooks 2004; Coniglio and Parker 2020) is tied to characteristics of the rear-flank outflow (e.g., Markowski et al. 2002; Kumjian 2011; French et al. 2015).

Of the kinematic and thermodynamic parameters tested in this study, peak low-level mesocyclone intensities were most strongly correlated with 0–3-km SRH and MLLCL, respectively. Thus, given an expected range of MLLCL and 0–3-km SRH values, this analysis provides an estimate of what AzShear values forecasters might "expect" from a mature low-level mesocyclone. For example, the mean, peak AzShear value for a low-level mesocyclone in an environment characterized by MLLCLs around 750–1000 m and 0–3-km SRH around 300–400 m^2 s^{-2} is roughly 0.017 s^{-1} (see the bin outlined in red in Fig. 5b). This differs from the mean, peak AzShear value for a low-level mesocyclone in an environment with MLLCLs around 1250–1500-m and 0–3-km SRH around 100–200 m^2 s^{-2}: around 0.012 s^{-1} (see the bin outlined in yellow in Fig. 5b). It is also possible to quantify the probability that a low-level mesocyclone strengthens or weakens during a subsequent time interval, given a range of initial mesocyclone strengths and general background environmental parameters. An example of two mesocyclones with initial AzShear values of 0.02 and 0.007 s^{-1}—residing in the higher-end MLLCL (750–1000 m) and 0–3-km SRH (300–400 m^2 s^{-2}) bins—is shown in Fig. 10. The violin in Fig. 10a shows the distribution of initial AzShear values for randomly selected 30-min periods of supercell life cycles within environments characterized by these MLLCL and 0–3-km SRH bins. The hypothetical initial AzShear values of 0.02 and 0.007 s^{-1} are shown in orange and magenta, respectively. The initial AzShear value 0.02 s^{-1} lies near the top of the violin, suggesting that this mesocyclone is "overperforming" and will likely weaken. The scatterplot in Fig. 10b quantifies this relationship. In this case, all points with initial AzShear within ±0.002 s^{-1} of the hypothetical AzShear value (e.g., 0.018–0.022 s^{-1}) weaken during the next 30 min, suggesting that this mesocyclone has essentially a 100% chance of weakening. The linear least squares regression line ($p = 0$ and $R^2 = 0.2966$) suggests that this mesocyclone may weaken by around 0.007 s^{-1}. In the same environment and using the same initial AzShear window of ±0.002 s^{-1}, an initial AzShear of 0.007 s^{-1} has a roughly 69% chance to strengthen during the next 30 min (by around 0.003 s^{-1} based on the regression).

The sample sizes for these probabilities in this study dwindle rapidly due to their dependence on both environmental

conditions and initial mesocyclone strength. This currently limits further potential real-time utility and warrants reservation about portions of the parameter spaces until more observations are collected (e.g., increasing the binned sample sizes in Figs. 5–7). Another limitation is that these findings are drawn from a sample of only tornadic and significant-severe supercells; the degree to which they are generalizable to nontornadic/nonsevere supercells remains uncertain until a larger, more diverse supercell dataset can be examined. The creation of such a dataset is planned in the near future that will address these limitations.

The finding that environmental kinematics are generally more strongly correlated with peak AzShear than thermodynamic parameters is consistent with prior observational work relating environmental conditions to supercell strength, at least in terms of tornadic production. Although the Thompson et al. (2003) dataset showed that significantly tornadic supercells tended to feature more supportive local thermodynamic conditions (like MLCAPE) than weakly tornadic supercells, the Rasmussen and Blanchard (1998) and Craven and Brooks (2004) studies showed similar CAPE distributions across the same supercell-tornado parameter space. Low-level kinematic characteristics exhibited a more consistent signal across these climatologies, featuring greater BWD and SRH for significantly tornadic supercell environments compared to weakly tornadic ones. This is consistent with our analysis, which is based not on tornado production but rather on explicit low-level mesocyclone intensity derived from WSR-88D observations. This result also suggests that—in line with recent idealized sensitivity studies (Coffer and Parker 2018; Flournoy et al. 2020)—mesocyclone evolution and tornado production in a background environment may be more sensitive to slight variations in the wind profile than the thermodynamic profile.

Along these lines, latitudinal, storm-scale datasets like the one analyzed in this study will be very useful for quantifying the range of outcomes (with respect to mesocyclone evolution and tornado production) that are possible in different background environments. This topic has been featured in a few recent idealized modeling studies (Coffer et al. 2017; Flournoy et al. 2020; Markowski 2020; Hutson and Weiss 2023), which currently have no observational complement (other than a few individual case studies; e.g., Klees et al. 2016; Wilson et al. 2023). We attempted to quantify the range of mesocyclone outcomes in this study with an approach similar to that in Figs. 5–7, e.g., computing the range of peak AzShear values in each environmental bin rather than the mean. The results suggest that as the mean peak intensity increases, so does the range of peak intensities observed across multiple supercells evolving in a similar parameter space (not shown). However, the range calculation can be quite sensitive to the number of observed mesocyclones in each bin; restricting the range analysis to bins with a sufficient number of mesocyclones (e.g., around 10 or more) limits the analyzed environmental parameter space, the resolution of any trends, and the generality of any trends that may exist.

7. Summary and concluding remarks

This study was motivated by recent work regarding the possible association of cell mergers with supercell mesocyclone evolution, as well as more detailed relationships between mesocyclone evolution and characteristics of the background environment. We integrated open questions related to these topics into a few primary areas of focus for our analysis:

- Do supercell mesocyclones tend to regress toward a given intensity? If so, over what time scales does this occur?
- Are mean mesocyclone intensities influenced by the background environment?
- Is mesocyclone evolution more strongly influenced by cell mergers in different environments?

We synthesized multiple databases—the F22 supercell dataset and SFCOA environmental reanalysis—to support a latitudinal examination of storm-scale mesocyclone evolutionary trends across hundreds of supercells. This yielded novel analyses of low-level mesocyclone characteristics in different environments, particularly with respect to temporal mesocyclone evolution. Responses to our research questions are summarized as follows:

- Across all environments, significant-supercell mesocyclones tended to regress toward an intensity characterized by maximum 0–3-km AzShear values around 0.01 s^{-1}. This occurs over all of the time scales that we analyzed (5–120 min), with the regression toward the mean becoming clearer over longer time periods. This is consistent with the idea that over time, mature supercell mesocyclones may reach a quasi-steady state, but short-term trends in mesocyclone evolution can be strongly influenced by factors not clearly related to the background environment.
- The expected intensities of mature, quasi-steady mesocyclones are (at least) a function of the simultaneous and recent background environment. In particular, mature, quasi-steady mesocyclone intensities varied consistently across the 0–3-km SRH–MLLCL parameter space, with greater 0–3-km SRH and lower MLLCLs favoring stronger peak mesocyclone intensities at the same time. Periods of peak mesocyclone intensity were also generally associated with antecedent 1-h increases in those same parameters. This begins to quantify the respective time scales over which environmental changes influence mesocyclone strength.
- The outcome of a cell merger, in terms of low-level mesocyclone evolution, is not strongly related to any of the tested environmental parameters. While the relationship between across-merger 0–3-km AzShear and MLLCL was statistically significant (at the 95% confidence level), the low R^2 value (0.0341) suggests that such a relationship is not currently useful for increasing predictive skill.

These findings are consistent with previous work relating characteristics of supercells to the background environments within which they reside. All of the summarized findings indicate that further analysis of observed mesocyclone evolution in different background environments would be beneficial, both for 1) extending results from recent idealized simulations to reality and 2) potential real-time forecast benefit. Among other aspects, findings from this vein of work should become increasingly relevant for quantifying the range of possible

mesocyclone evolutionary paths on any given day; such a quantification will readily increase the applicability of idealized-simulation sensitivity studies, provide a first guess at the desired dispersiveness for ensemble-based, short-term experimental guidance like the Warn-on-Forecast System (Stensrud et al. 2009, 2013; Heinselman et al. 2024), and support real-time prediction from subhourly to weekly time scales. To this end, a collaborative effort is currently underway to produce a database of thousands of observed, quality-controlled supercell tracks from initiation to demise across the contiguous United States. We hope that the analysis of such a dataset and other research avenues will extend these findings, as well as shed light on additional outstanding questions related to observed supercell evolution.

Acknowledgments. This work benefited from conversations with many scientists at the National Severe Storms Laboratory, Cooperative Institute for Severe and High-Impact Weather Research and Operations, and Storm Prediction Center, including but not limited to Makenzie Krocak, Israel Jirak, Mike Coniglio, Morgan Schneider, Lauren Pounds, Andrew Muehr, and Patrick Marsh. We thank the coauthors of F22 for their time and effort spent creating the dataset analyzed in this study. Finally, we thank Chris Weiss for managing this paper and are especially grateful for the suggestions from Casey Davenport, Brice Coffer, and an anonymous reviewer that greatly improved its quality. Andy Wade and Tony Lyza were supported through NOAA/Office of Oceanic and Atmospheric Research under the NOAA-University of Oklahoma Cooperative Agreement NA21OAR4320204, U.S. Department of Commerce. The statements, findings, conclusions, and recommendations are those of the authors and do not necessarily reflect the views of NOAA or the U.S. Department of Commerce.

Data availability statement. The supercell time series, associated SFCOA parameters, and analysis codes are available in an online GitHub repository at https://github.com/mdflournoy/supercell-environment-analysis. The MYRORSS database is publicly available at https://osf.io/9gzp2/.

REFERENCES

Adlerman, E. J., K. K. Droegemeier, and R. Davies-Jones, 1999: A numerical simulation of cyclic mesocyclogenesis. *J. Atmos. Sci.*, **56**, 2045–2069, https://doi.org/10.1175/1520-0469(1999)056<2045:ANSOCM>2.0.CO;2.

Barnes, S. L., 1973: Mesoscale objective analysis using weighted time-series observations. NOAA/National Severe Storms Laboratory Tech. Memo. ERL NSSL-62, 60 pp., https://repository.library.noaa.gov/view/noaa/17647/noaa_17647_DS1.pdf.

Bothwell, P. D., J. A. Hart, and R. L. Thompson, 2002: An integrated three-dimensional objective analysis scheme in use at the Storm Prediction Center. Preprints, *21st Conf. on Severe Local Storms/19th Conf. on Weather Analysis and Forecasting/15th Conf. on Numerical Weather Prediction*, San Antonio, TX, Amer. Meteor. Soc., JP3.1, https://ams.confex.com/ams/pdfpapers/47482.pdf.

Brooks, H. E., 2013: Severe thunderstorms and climate change. *Atmos. Res.*, **123**, 129–138, https://doi.org/10.1016/j.atmosres.2012.04.002.

Brown, M. C., and C. J. Nowotarski, 2019: The influence of lifting condensation level on low-level outflow and rotation in simulated supercell thunderstorms. *J. Atmos. Sci.*, **76**, 1349–1372, https://doi.org/10.1175/JAS-D-18-0216.1.

Bunkers, M. J., M. R. Hjelmfelt, and P. L. Smith, 2006: An observational examination of long-lived supercells. Part I: Characteristics, evolution, and demise. *Wea. Forecasting*, **21**, 673–688, https://doi.org/10.1175/WAF949.1.

Coffer, B. E., and M. D. Parker, 2015: Impacts of increasing low-level shear on supercells during the early evening transition. *Mon. Wea. Rev.*, **143**, 1945–1969, https://doi.org/10.1175/MWR-D-14-00328.1.

——, and ——, 2017: Simulated supercells in nontornadic and tornadic VORTEX2 environments. *Mon. Wea. Rev.*, **145**, 149–180, https://doi.org/10.1175/MWR-D-16-0226.1.

——, and ——, 2018: Is there a "tipping point" between simulated nontornadic and tornadic supercells in VORTEX2 environments? *Mon. Wea. Rev.*, **146**, 2667–2693, https://doi.org/10.1175/MWR-D-18-0050.1.

——, ——, J. M. L. Dahl, L. J. Wicker, and A. J. Clark, 2017: Volatility of tornadogenesis: An ensemble of simulated nontornadic and tornadic supercells in VORTEX2 environments. *Mon. Wea. Rev.*, **145**, 4605–4625, https://doi.org/10.1175/MWR-D-17-0152.1.

——, ——, J. M. Peters, and A. R. Wade, 2023: Supercell low-level mesocyclones: Origins of inflow and vorticity. *Mon. Wea. Rev.*, **151**, 2205–2232, https://doi.org/10.1175/MWR-D-22-0269.1.

Coniglio, M. C., 2012: Verification of RUC 0–1-h forecasts and SPC mesoscale analyses using VORTEX2 soundings. *Wea. Forecasting*, **27**, 667–683, https://doi.org/10.1175/WAF-D-11-00096.1.

——, and M. D. Parker, 2020: Insights into supercells and their environments from three decades of targeted radiosonde observations. *Mon. Wea. Rev.*, **148**, 4893–4915, https://doi.org/10.1175/MWR-D-20-0105.1.

——, and R. E. Jewell, 2022: SPC mesoscale analysis compared to field-project soundings: Implications for supercell environment studies. *Mon. Wea. Rev.*, **150**, 567–588, https://doi.org/10.1175/MWR-D-21-0222.1.

Craven, J. P., and H. E. Brooks, 2004: Baseline climatology of sounding derived parameters associated with deep, moist convection. *Natl. Wea. Dig.*, **28**, 13–24.

Dahl, J. M. L., 2017: Tilting of horizontal shear vorticity and the development of updraft rotation in supercell thunderstorms. *J. Atmos. Sci.*, **74**, 2997–3020, https://doi.org/10.1175/JAS-D-17-0091.1.

Davenport, C. E., 2021: Environmental evolution of long-lived supercell thunderstorms in the Great Plains. *Wea. Forecasting*, **36**, 2187–2209, https://doi.org/10.1175/WAF-D-21-0042.1.

Davies-Jones, R., 1984: Streamwise vorticity: The origin of updraft rotation in supercell storms. *J. Atmos. Sci.*, **41**, 2991–3006, https://doi.org/10.1175/1520-0469(1984)041<2991:SVTOOU>2.0.CO;2.

——, 2002: Linear and nonlinear propagation of supercell storms. *J. Atmos. Sci.*, **59**, 3178–3205, https://doi.org/10.1175/1520-0469(2003)059<3178:LANPOS>2.0.CO;2.

Dennis, E. J., and M. R. Kumjian, 2017: The impact of vertical wind shear on hail growth in simulated supercells. *J. Atmos. Sci.*, **74**, 641–663, https://doi.org/10.1175/JAS-D-16-0066.1.

Dowell, D. C., and H. B. Bluestein, 2002a: The 8 June 1995 McLean, Texas, storm. Part I: Observations of cyclic tornadogenesis. *Mon. Wea. Rev.*, **130**, 2626–2648, https://doi.org/10.1175/1520-0493(2002)130<2626:TJMTSP>2.0.CO;2.

——, and ——, 2002b: The 8 June 1995 McLean, Texas, storm. Part II: Cyclic tornado formation, maintenance, and dissipation. *Mon. Wea. Rev.*, **130**, 2649–2670, https://doi.org/10.1175/1520-0493(2002)130<2649:TJMTSP>2.0.CO;2.

Edwards, R., and R. L. Thompson, 2024: Right-moving supercell tornadogenesis during interaction with a left-moving supercell's rear-flank outflow. *Wea. Forecasting*, **39**, 141–153, https://doi.org/10.1175/WAF-D-23-0075.1.

Fischer, J., and J. M. L. Dahl, 2023: Supercell-external storms and boundaries acting as catalysts for tornadogenesis. *Mon. Wea. Rev.*, **151**, 23–38, https://doi.org/10.1175/MWR-D-22-0026.1.

——, M. D. Flournoy, and A. W. Lyza, 2023: Comments on "a climatology of cell mergers with supercells and their association with mesocyclone evolution" and "the influence of cell mergers on supercell characteristics and tornado evolution on 27–28 April 2011". *Mon. Wea. Rev.*, **151**, 2541–2545, https://doi.org/10.1175/MWR-D-23-0120.1.

Flournoy, M. D., M. C. Coniglio, E. N. Rasmussen, J. C. Furtado, and B. E. Coffer, 2020: Modes of storm-scale variability and tornado potential in VORTEX2 near- and far-field tornadic environments. *Mon. Wea. Rev.*, **148**, 4185–4207, https://doi.org/10.1175/MWR-D-20-0147.1.

——, ——, and ——, 2021: Examining relationships between environmental conditions and supercell motion in time. *Wea. Forecasting*, **36**, 737–755, https://doi.org/10.1175/WAF-D-20-0192.1.

——, A. W. Lyza, M. A. Satrio, M. R. Diedrichsen, M. C. Coniglio, and S. Waugh, 2022: A climatology of cell mergers with supercells and their association with mesocyclone evolution. *Mon. Wea. Rev.*, **150**, 451–461, https://doi.org/10.1175/MWR-D-21-0204.1.

French, M. M., D. W. Burgess, E. R. Mansell, and L. J. Wicker, 2015: Bulk hook echo raindrop sizes retrieved using mobile, polarimetric Doppler radar observations. *J. Appl. Meteor. Climatol.*, **54**, 423–450, https://doi.org/10.1175/JAMC-D-14-0171.1.

Goldacker, N. A., and M. D. Parker, 2021: Low-level updraft intensification in response to environmental wind profiles. *J. Atmos. Sci.*, **78**, 2763–2781, https://doi.org/10.1175/JAS-D-20-0354.1.

Gropp, M. E., and C. E. Davenport, 2018: The impact of the nocturnal transition on the lifetime and evolution of supercell thunderstorms in the Great Plains. *Wea. Forecasting*, **33**, 1045–1061, https://doi.org/10.1175/WAF-D-17-0150.1.

Hastings, R., and Y. Richardson, 2016: Long-term morphological changes in simulated supercells following mergers with nascent supercells in directionally varying shear. *Mon. Wea. Rev.*, **144**, 471–499, https://doi.org/10.1175/MWR-D-15-0193.1.

Hastings, R. M., Y. P. Richardson, and P. M. Markowski, 2014: Simulation of near-surface mesocyclogenesis during mergers between mature and nascent supercells. *27th Conf. on Severe Local Storms*, Madison, WI, Amer. Meteor. Soc., 3B.2, https://ams.confex.com/ams/27SLS/webprogram/Manuscript/Paper255837/RyanHastings_extended_abstract.pdf.

Heinselman, P. L., and Coauthors, 2024: Warn-on-forecast system: From vision to reality. *Wea. Forecasting*, **39**, 75–95, https://doi.org/10.1175/WAF-D-23-0147.1.

Hutson, A., and C. Weiss, 2023: Using ensemble sensitivity analysis to identify storm characteristics associated with tornadogenesis in high resolution simulated supercells. *Mon. Wea. Rev.*, **151**, 2633–2658, https://doi.org/10.1175/MWR-D-22-0288.1.

Jewett, B. F., R. W. Przybylinski, and R. B. Wilhelmson, 2006: Numerical simulation of the 24 April, 2002 storm merger between a left-moving storm and a supercell. *23rd Conf. on Severe Local Storms*, St. Louis, MO, Amer. Meteor. Soc., P11.3, https://ams.confex.com/ams/23SLS/techprogram/paper_115478.htm.

Katona, B., and P. Markowski, 2021: Assessing the influence of complex terrain on severe convective environments in northeastern Alabama. *Wea. Forecasting*, **36**, 1003–1029, https://doi.org/10.1175/WAF-D-20-0136.1.

Klees, A. M., Y. P. Richardson, P. M. Markowski, C. Weiss, J. M. Wurman, and K. K. Kosiba, 2016: Comparison of the tornadic and nontornadic supercells intercepted by VORTEX2 on 10 June 2010. *Mon. Wea. Rev.*, **144**, 3201–3231, https://doi.org/10.1175/MWR-D-15-0345.1.

Kumjian, M. R., 2011: Precipitation properties of supercell hook echoes. *Electron. J. Severe Storms Meteor.*, **6** (5), https://ejssm.org/archives/wp-content/uploads/2021/09/vol6-5.pdf.

Lee, B. D., B. F. Jewett, and R. B. Wilhelmson, 2006: The 19 April 1996 Illinois tornado outbreak. Part II: Cell mergers and associated tornado incidence. *Wea. Forecasting*, **21**, 449–464, https://doi.org/10.1175/WAF943.1.

Lyza, A. W., and K. R. Knupp, 2018: A background investigation of tornado activity across the Southern Cumberland Plateau terrain system of Northeastern Alabama. *Mon. Wea. Rev.*, **146**, 4261–4278, https://doi.org/10.1175/MWR-D-18-0300.1.

——, and M. D. Flournoy, 2023: The influence of cell mergers on supercell characteristics and tornado evolution on 27–28 April 2011. *Mon. Wea. Rev.*, **151**, 1551–1569, https://doi.org/10.1175/MWR-D-22-0189.1.

——, T. A. Murphy, B. T. Goudeau, P. T. Pangle, K. R. Knupp, and R. A. Wade, 2020: Observed near-storm environment variations across the southern Cumberland Plateau system in northeastern Alabama. *Mon. Wea. Rev.*, **148**, 1465–1482, https://doi.org/10.1175/MWR-D-19-0190.1.

Magee, K. M., and C. E. Davenport, 2020: An observational analysis quantifying the distance of supercell-boundary interactions in the Great Plains. *J. Oper. Meteor.*, **8**, 15–38, https://doi.org/10.15191/nwajom.2020.0802.

Mahalik, M. C., B. R. Smith, K. L. Elmore, D. M. Kingfield, K. L. Ortega, and T. M. Smith, 2019: Estimates of gradients in radar moments using a linear least squares derivative technique. *Wea. Forecasting*, **34**, 415–434, https://doi.org/10.1175/WAF-D-18-0095.1.

Markowski, P. M., 2020: What is the intrinsic predictability of tornadic supercell thunderstorms? *Mon. Wea. Rev.*, **148**, 3157–3180, https://doi.org/10.1175/MWR-D-20-0076.1.

——, and Y. P. Richardson, 2014: The influence of environmental low-level shear and cold pools on tornadogenesis: Insights from idealized simulations. *J. Atmos. Sci.*, **71**, 243–275, https://doi.org/10.1175/JAS-D-13-0159.1.

——, J. M. Straka, and E. N. Rasmussen, 2002: Direct surface thermodynamic observations within the rear-flank downdrafts of nontornadic and tornadic supercells. *Mon. Wea. Rev.*, **130**, 1692–1721, https://doi.org/10.1175/1520-0493(2002)130<1692:DSTOWT>2.0.CO;2.

Moller, A. R., C. A. Doswell III, M. P. Foster, and G. R. Woodall, 1994: The operational recognition of supercell thunderstorm environments and storm structures. *Wea. Forecasting*, **9**, 327–347, https://doi.org/10.1175/1520-0434(1994)009<0327:TOROST>2.0.CO;2.

Muehr, A. J., J. H. Ruppert, M. D. Flournoy, and J. M. Peters, 2024: The influence of midlevel shear and horizontal rotors on supercell updraft dynamics. *J. Atmos. Sci.*, **81**, 153–176, https://doi.org/10.1175/JAS-D-23-0082.1.

Nielsen, E. R., and R. S. Schumacher, 2018: Dynamical insights into extreme short-term precipitation associated with supercells and mesovortices. *J. Atmos. Sci.*, **75**, 2983–3009, https://doi.org/10.1175/JAS-D-17-0385.1.

Parker, M. D., 2014: Composite VORTEX2 supercell environments from near-storm soundings. *Mon. Wea. Rev.*, **142**, 508–529, https://doi.org/10.1175/MWR-D-13-00167.1.

——, 2017: How much does "backing aloft" actually impact a supercell? *Wea. Forecasting*, **32**, 1937–1957, https://doi.org/10.1175/WAF-D-17-0064.1.

Peters, J. M., C. J. Nowotarski, and H. Morrison, 2019: The role of vertical wind shear in modulating maximum supercell updraft velocities. *J. Atmos. Sci.*, **76**, 3169–3189, https://doi.org/10.1175/JAS-D-19-0096.1.

Púčik, T., and Coauthors, 2017: Future changes in European severe convection environments in a regional climate model ensemble. *J. Climate*, **30**, 6771–6794, https://doi.org/10.1175/JCLI-D-16-0777.1.

Rasmussen, E. N., and D. O. Blanchard, 1998: A baseline climatology of sounding-derived supercell and tornado forecast parameters. *Wea. Forecasting*, **13**, 1148–1164, https://doi.org/10.1175/1520-0434(1998)013<1148:ABCOSD>2.0.CO;2.

Rogers, J. W., 2012: Significant tornado events associated with cell mergers. *26th Conf. on Severe Local Storms*, Nashville, TN, Amer. Meteor. Soc., 9.4, https://www.spc.noaa.gov/publications/rogers/mergers.pdf.

——, and C. C. Weiss, 2008: The association of cell mergers with tornado occurrence. *24th Conf. on Severe Local Storms*, Savannah, GA, Amer. Meteor. Soc., P3.23, https://ams.confex.com/ams/pdfpapers/141784.pdf.

Rotunno, R., and J. B. Klemp, 1982: The influence of the shear-induced pressure gradient on thunderstorm motion. *Mon. Wea. Rev.*, **110**, 136–151, https://doi.org/10.1175/1520-0493(1982)110<0136:TIOTSI>2.0.CO;2.

——, and J. Klemp, 1985: On the rotation and propagation of simulated supercell thunderstorms. *J. Atmos. Sci.*, **42**, 271–292, https://doi.org/10.1175/1520-0469(1985)042<0271:OTRAPO>2.0.CO;2.

Smith, B. T., R. L. Thompson, J. S. Grams, C. Broyles, and H. E. Brooks, 2012: Convective modes for significant severe thunderstorms in the contiguous United States. Part I: Storm classification and climatology. *Wea. Forecasting*, **27**, 1114–1135, https://doi.org/10.1175/WAF-D-11-00115.1.

Stensrud, D. J., and Coauthors, 2009: Convective-scale warn-on-forecast system. *Bull. Amer. Meteor. Soc.*, **90**, 1487–1500, https://doi.org/10.1175/2009BAMS2795.1.

——, and Coauthors, 2013: Progress and challenges with warn-on-forecast. *Atmos. Res.*, **123**, 2–16, https://doi.org/10.1016/j.atmosres.2012.04.004.

Tanamachi, R. L., P. L. Heinselman, and L. J. Wicker, 2015: Impacts of a storm merger on the 24 May 2011 El Reno, Oklahoma, tornadic supercell. *Wea. Forecasting*, **30**, 501–524, https://doi.org/10.1175/WAF-D-14-00164.1.

Taszarek, M., J. T. Allen, H. E. Brooks, N. Pilguj, and B. Czernecki, 2021: Differing trends in United States and European severe thunderstorm environments in a warming climate. *Bull. Amer. Meteor. Soc.*, **102**, E296–E322, https://doi.org/10.1175/BAMS-D-20-0004.1.

Thompson, R. L., R. Edwards, J. A. Hart, K. L. Elmore, and P. Markowski, 2003: Close proximity soundings within supercell environments obtained from the rapid update cycle. *Wea. Forecasting*, **18**, 1243–1261, https://doi.org/10.1175/1520-0434(2003)018<1243:CPSWSE>2.0.CO;2.

——, C. M. Mead, and R. Edwards, 2007: Effective storm-relative helicity and bulk shear in supercell thunderstorm environments. *Wea. Forecasting*, **22**, 102–115, https://doi.org/10.1175/WAF969.1.

Warren, R. A., H. Richter, H. A. Ramsay, S. T. Siems, and M. J. Manton, 2017: Impact of variations in upper-level shear on simulated supercells. *Mon. Wea. Rev.*, **145**, 2659–2681, https://doi.org/10.1175/MWR-D-16-0412.1.

Williams, S. S., K. L. Ortega, T. M. Smith, and A. E. Reinhart, 2022: Comprehensive radar data for the contiguous United States: Multi-year reanalysis of remotely sensed storms. *Bull. Amer. Meteor. Soc.*, **103**, E838–E854, https://doi.org/10.1175/BAMS-D-20-0316.1.

Wilson, M. B., and Coauthors, 2023: Environmental and storm-scale controls on close proximity supercells observed by TORUS on 8 June 2019. *Mon. Wea. Rev.*, **151**, 3013–3035, https://doi.org/10.1175/MWR-D-23-0002.1.

Wurman, J., Y. Richardson, C. Alexander, S. Weygandt, and P. F. Zhang, 2007: Dual-Doppler and single-Doppler analysis of a tornadic storm undergoing mergers and repeated tornadogenesis. *Mon. Wea. Rev.*, **135**, 736–758, https://doi.org/10.1175/MWR3276.1.